Earth-Science Reviews 162 (2016) 129–154

Contents lists available at ScienceDirect

Earth-Science Reviews

journal homepage: www.elsevier.com/locate/earscirev

Invited review

Evaluating the life expectancy of a desert pavement

Yeong Bae Seong [a,*], Ronald I. Dorn [b], Byung Yong Yu [c]

[a] Department of Geography Education, Korea University, Seoul 136-701, Republic of Korea
[b] School of Geographical Sciences & Urban Planning, Arizona State University, Tempe, AZ 85287-5302, USA
[c] AMS Laboratory, Advanced Analysis Center, Korea Institute of Science and Technology, Seoul 136-791, Republic of Korea

ARTICLE INFO

Article history:
Received 26 April 2016
Received in revised form 9 August 2016
Accepted 9 August 2016
Available online 14 August 2016

Keywords:
Cosmogenic nuclides
Geomorphology
Landform evolution
Quaternary
Soils

ABSTRACT

This paper integrates prior scholarship on desert pavements with a case study of pavements on stream terraces in the Sonoran Desert to analyze the processes and site conditions that facilitate the survival of ancient desert pavements. This synthesis identifies vital factors, key factors, and site-specific factors promoting pavement stability. Hyperaridity is the vital factor in pavements surviving for 10^6 years or more, aided by minimal bioturbation and clast-size reduction. Three key factors aid in pavements surviving for 10^4 to 10^5 years: accumulation of allochthonous dust underneath pavement cobbles; a flat topography; and a lack of headward retreating swales or gullies. A unified explanation for pavement longevity, however, did not emerge from a literature review, because a variety of site-specific factors can also promote pavement antiquity including: resistant bedrock beneath the pavement; disk-shaped cobbles to promote dust accumulation; and microclimatological and ecological reasons for minimal bioturbation. Both key and site-specific explanations for pavement longevity apply well to a case study of pavements on stream terraces in the Sonoran Desert, central Arizona. The buildup of cosmogenic ^{10}Be and *in situ* ^{14}C, optically stimulated luminescence and varnish microlamination ages reveal stable pavements range in age between ~30 and 332 ka with conditions for longevity including: flat surface topography; pavements underlain by consolidated granitic bedrock; a lack of headward-retreating gullies and swales; ^{87}Sr/^{86}Sr analyses indicating the infiltration of allochthonous dust floating disk-shaped pavement cobbles; and a quartzite lithology resistant to disintegration. However, ^{10}Be ages also indicate evidence for the instability of desert pavements on stream terraces underlain by unconsolidated playa clays and unconsolidated fanglomerate; these weaker materials allowed the growth of headward-retreating swales, that in turn promoted exposure of newer gravels by surface erosion.

Contents

* Corresponding author.
E-mail addresses: ybseong@korea.ac.kr, ybseong@hotmail.com (Y.B. Seong).

http://dx.doi.org/10.1016/j.earscirev.2016.08.005
0012-8252/

1. Introduction

Desert pavement consists of a gravel surface one or two stones thick (Mabbutt, 1965; Cooke, 1970; Mabbutt, 1979) that occurs in both cold (Bockheim, 2010) and warm (Dixon, 2009) deserts. This paper focuses on warm desert pavements that go by a variety of names (Cooke and Warren, 1973; Mabbutt, 1977): desert pavement in North and South America, as well as India (Moharana and Raja, 2016); reg for smaller gravels in the western Sahara and Middle East; hamada for residual rocks or boulders forming the surface of a rocky tableland in the western Sahara and Middle East; serir in the central Sahara where stones are larger than regs; gibber (or stony desert) in Australia; saï in the Tarim Desert; and the Mongol term gobi for pebbly-rocky plains in central Asia. Stony mantles (Laity, 2011) and stone pavements (Dietze and Kleber, 2012) are sometimes used as synonyms, while some archaeologists use stone mulches in place of desert pavements (Aerts et al., 2010). For the sake of consistency, we employ the terms desert pavement or just pavement throughout. Fig. 1 presents examples from various warm deserts.

While much has been written about desert pavements in the past few decades (Dixon, 2009; Laity, 2011), this review focuses on factors promoting desert pavement longevity. We start by presenting a literature review. However, a literature review alone does not fully communicate our thesis that pavement stability can be the result of a complex mix of general factors (*e.g.* hyper-aridity, allochthonous dust floating a pavement, flat topography) and site-specific factors. Thus, we also contextualize prior scholarship by presenting a case study of new research on the oldest known (yet) desert pavement in the Sonoran Desert, North America, to further elucidate reasons for the longevity of desert pavements.

2. Literature overview of warm desert pavements

2.1. Why ancient pavements are important

Desert pavements develop on a wide array of landforms (Table 1). Measuring pavement age provides insight into the antiquity of the underlying landform. Pavement age is also a concern to academic scholarship in a variety of earth-science fields beyond geomorphology including: geoarchaeology, geochemistry, hydrology, paleoseismology, physical geography, Quaternary Research, soil science, and surficial geology. Desert pavement stability can also play a role in applied earth-science research, because the placement of the hazardous waste of our modern society often requires a stable setting (Stirling et al., 2010; Wright et al., 2014; Potter, 2016).

The existence of an ancient stable pavement provides a platform for the preservation of a diverse array of materials such as ancient artifacts (Adelsberger and Smith, 2009; Latorre et al., 2013; Honegger and Williams, 2015) and meteorite fragments (Kring et al., 2001). Post-depositional changes to artifacts in desert pavements can be useful in assigning relative, correlated, and calibrated ages (Hunt, 1960; Hayden, 1976; Frink and Dorn, 2001; Cerveny et al., 2006; Zerboni, 2008; Adelsberger et al., 2013; Baied and Somonte, 2013; Ugalde et al., 2015). Geoglyphs are constructed into desert pavement, such as the Nasca lines in Peru (Wagner and Kadereit, 2010), alignments in North America (Cerveny et al., 2006), and the geometric lines in the Arabian Desert (Athanassas et al., 2015).

Desert pavements are generally considered an indicator of aridity (Pietsch and Kuhn, 2012; Fitzsimmons et al., 2013). Pavement antiquity can provide important evidence for the timing of major climatic transitions, to when a desert region became arid enough to preserve a desert pavement. For example, desert pavement did not develop in southern Arabia until regional desiccation initiated in the early Holocene (Pietsch and Kuhn, 2012). Desert pavements also record the onset of hyperaridity on timescales of 10^6 years, for the Atacama Desert (Dunai et al., 2005; Nishiizumi et al., 2005; Evenstar et al., 2009; Wang et al., 2015), the gibber plains in Australia (Fujioka et al., 2005), the Gobi Desert (Lv et al., 2010), and the southern Levant (Amit et al., 2011).

Some argue that buried pavements in warm deserts have potential for use as a paleoenvironmental indicator of aridity or rates of dust accumulation (Dorn and Dickinson, 1989; Marchant and Denton, 1996; Field et al., 2002; Dietze et al., 2011, 2012, 2013, 2016). An important distinction exists, however, between buried pavements in desert regions and buried stone lines in the wet tropics that have sometimes been termed buried desert pavements (Colinvaux et al., 2000). These buried stone lines found in temperate and tropical humid areas are not buried desert pavements, but they result of complex bioturbation processes (Johnson, 1989, 1990; Johnson and Balek, 1991).

Desert pavement antiquity plays a role in understanding desert soils and desert biota (Peterson, 1981; Peterson et al., 1995; McFadden et al., 1998; Young et al., 2004; Wood et al., 2005). For example, studies of the fallout ^{137}Cs in soil profiles indicates that clay particles that bind ^{137}Cs are transported through soil profiles by infiltration and not bioturbation (Pelletier et al., 2005). The highest biodiversity tends to exist before smooth pavements form, but biodiversity declines as pavements change soil water-holding capacity and infiltration capacity (Shafer et al., 2004).

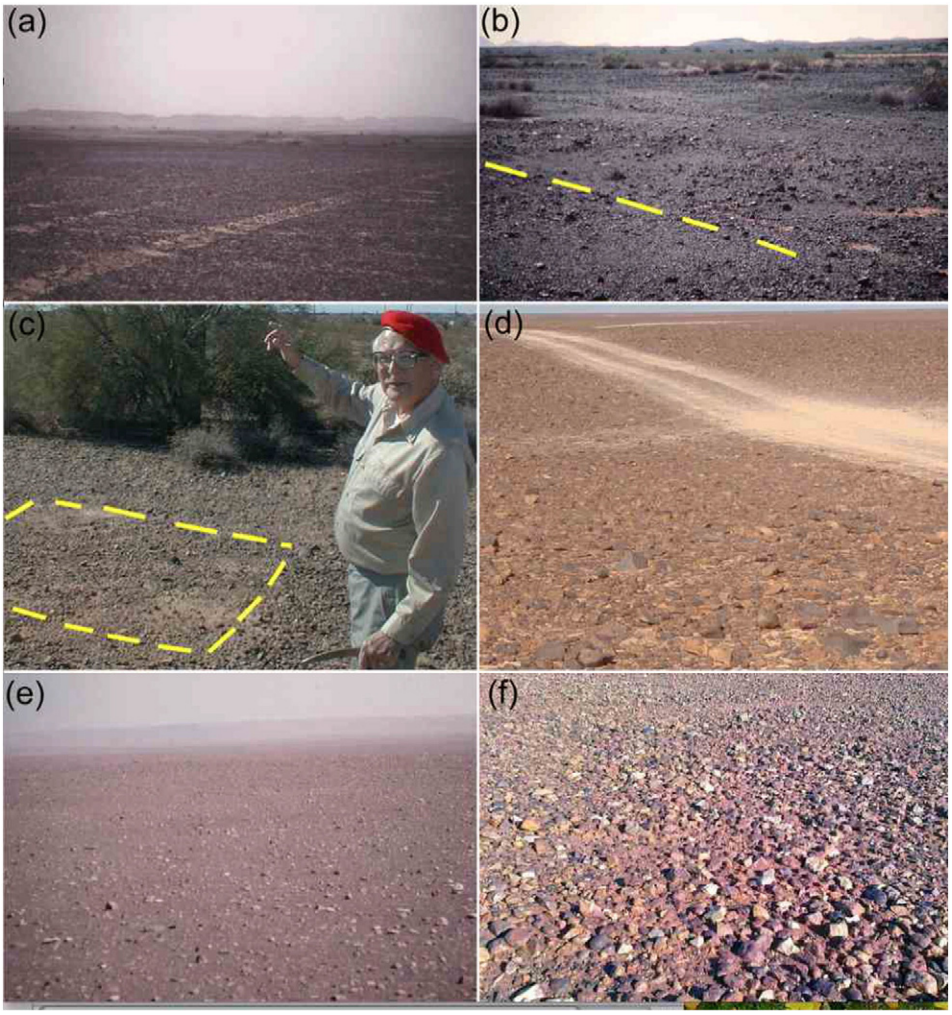

Fig. 1. Desert pavements around the globe (a) reg in the southern Levant Desert, Israel with 15-year old tank tracks for scale; (b) in the Sierra Pinacate Mexico, with an early Holocene trail (Hayden, 1976) for scale adjacent to the dashed line; (c) healing of a desert pavement 24 years after scraping, Mesa, Arizona (Péwé, 1978); (d) hamadas on Messak Settafet (earthobservatory.nasa.gov/IOTD/view.php?id=86118), Libya with road for scale; (e) deflation pavement of the Rio Grande, Peru (S 14.79102; W 75.3905), with image foreground 10 m wide; (f) gibbers near Coober Pedy, Australia with image foreground 5 m wide.

Hence, old pavements impact ecological patterns in the Sonoran (McAuliffe, 1994) and the Mojave (Pietrasiak et al., 2014) deserts of North America.

2.2. Factors promoting the formation of desert pavements

Since pavement longevity involves factors related to pavement genesis, this section reviews current scholarship on birthing processes. Desert pavements require certain geomorphic and vegetative settings before they can develop. Potential pavements require a surface not subject to gullying from overland flow (Peel, 1960; Cooke, 1970; Huang et al., 2014), have low slope angles (Ugolini et al., 2008), and have dry enough conditions to inhibit bioturbation (Pietrasiak et al., 2014).

A clear distinction exists between deflation and non-deflation pavements, and this paper focuses pavements that do not form as a result of wind concentrating cobbles at the surface by transporting sand and dust. Still, it is important to review some of the recent deflation pavement literature, in part because persistent examples exist of deflation producing pavements that are (a) not coated in rock varnish, (b) do not have vesicular Av soil horizons underneath surface clasts, (c) have more widely spaced clasts separated by a sandy surface, (d) often occur near aeolian sands, and (e) where the clasts are clearly wind abraded (Symmons and Hemming, 1968; Cooke and Warren, 1973; Grolier et al., 1974; Goudie and Wilkinson, 1977; Williams and Greeley, 1984; Breed et al., 1989; Thomas et al., 2005; Wang et al., 2006; Al-Farraj, 2008; Dortch and Schoenbohm, 2011; Hussain and Aghwan, 2014; Zhang et al., 2014).

Deflation pavements stabilize sand in the Libyan Sahara (Bubenzer et al., 2007), in the Gobi Desert, China (Brookes, 2001; Jianjun et al., 2001; Wang et al., 2006; Zhang et al., 2014), and in Iran (Kianian, 2014). Deflation pavements can result from accelerated erosion of an A-horizon in semi-arid Patagonia, Argentina (Rostagno and Degorgueb, 2011), and studies from Fuego-Patagonia suggest that deflation can alter the characteristics of desert pavements (Borrazzo, in press). Cosmogenic ^{10}Be accumulations in surface cobbles and depth profiles in the Andean Precordillera are consistent with pavement formation by deflation sometime in the past (Siame et al., 1997; Schmidt et al., 2011).

A complication exists in trying to distinguish deflation pavements from non-deflation pavements where climatic change reduces aeolian abrasion. A reduction in aeolian activity permits the formation of rock varnish on ventifacts (Dorn, 1986), and can also promote the accumulation of dust underneath surface cobbles. For example, periodic aeolian deflation helps winnow fines away from desert pavements in the hyperarid Precordillera of Argentina (Hedrick et al., 2013), even though this deflation must be inactive at present because of the strong presence of rock varnish that would be abraded if deflation was active (Dorn and Oberlander, 1982). In Dakhla Oasis Region in Egypt the pavement was

Table 1
Studies where desert pavements provide age control for the underlying landform.

Host landform	Setting	References
Alluvial fan or plain	Arid Andes Mountains	Siame et al. (1997)
	Atacama Desert, Chile	Nishiizumi et al. (2005), Gonzalez et al. (2006), Cortes et al. (2012) Placzek et al. (2014), Wang et al. (2015)
	Central Asia	Hetzel et al. (2004), Lv et al. (2010)
	Dead Sea	LeBeon et al. (2010)
	Great Basin, USA	Reheis et al. (1992), Nishiizumi et al. (1993), Peterson et al. (1995), Duhnforth et al. (2007), Frankel et al. (2007a, 2007b); Sohn et al. (2007), Machette et al. (2008), Owen et al. (2011), Dickerson et al. (2013), Ivy-Ochs et al. (2013), Liu and Broecker (2013), Dickerson and Cocks (2015)
	Iranian Desert	Regard et al. (2006)
	Mojave Desert, USA	Ku et al. (1979), McDonald et al. (2003), Oskin et al. (2007), Cyr et al. (2010)
	Sonoran Desert, North America	Huckleberry (1993, 1994), Van Der Woerd et al. (2006), Spelz et al. (2008), Blisniuk et al. (2010), Blisniuk et al. (2012), Fenton and Pelletier (2013), Gray et al. (2014), Wright et al. (2014)
Basalt flow	Canary Islands	Dunai and Wijbrans (2000)
	Colorado Plateau, USA	Fenton and Niedermann (2014)
	Great Basin, USA	Zreda et al. (1993), Peterson et al. (1995), Shepard et al. (1995), Heizler et al. (1999), Valentine and Harrington (2006), Valentine et al. (2006)
	Jordan	Fuchs et al. (in press)
	Mojave Desert, USA	Turrin et al. (1985), Wells et al. (1985), McFadden et al. (1987), McFadden et al. (1998), Dietze et al. (2016)
Lake beach ridge or shoreline	Arid Australia	Al-Farraj (2008), May et al. (2015)
	Great Basin, USA	Nishiizumi et al. (1993), Duhnforth et al. (2007), Frankel et al. (2007a, 2007b); Machette et al. (2008), Owen et al. (2011), Ivy-Ochs et al. (2013)
	Mojave Desert, USA	Meek (1989, 1990, 2004), Reheis and Edwine (2008)
	Dead Sea	Liu et al. (2013)
Bedrock plateau	Arid Australia	Fujioka et al. (2005)
	Great Basin, USA	Goethals et al. (2007)
	Negev Desert Israel	Boroda et al. (2014)
	Sahara Desert	Adelsberger and Smith (2009)
Debris flows	Colorado Plateau	Marchetti and Cerling (2005)
	Great Basin, USA	Mihir et al. (2015)
Glacial deposits	Andes Mountains	Ward et al. (2015)
	Antarctica	Marchant et al. (1993), Marchant and Denton (1996), Marchant et al. (1996), Bockheim (2010)
	Xinjiang Province, China	Owen et al. (2012)
Marine terrace	Atacama Desert	Rodriguez et al. (2013b)
Pediment	Atacama Desert	Hall et al. (2008), Evenstar et al. (2009), Rodriguez et al. (2013b)
	Australia	Fisher et al. (2014)
Stream terrace - fill	Arabian Desert	Al-Farraj and Harvey (2000)
	Atacama Desert, Chile	Amundson et al. (2012), Jungers et al. (2013)
	Colorado Plateau, USA	Fenton et al. (2002), Fenton et al. (2004), Anders et al. (2005), Marchetti and Cerling (2005), Hidy et al. (2010)
	Negev Desert	Guralnik et al. (2011)
Steram terrace - strath	Andean Precordillera Argentina	Schmidt et al. (2011), Hedrick et al. (2013), Siame et al. (2015)
	Mojave Desert, USA	Meek (2004), Cyr et al. (2015)
	Rocky Mountains, USA	Anderson et al. (1996)
	Sonoran Desert	Armstrong et al. (2010), Larson et al. (2010)
	Tian Shan, China	Huang et al. (2014)
	Tibet	Perrineau et al. (2011), Shirahama et al. (2015)
Talus flatiron	Negev Desert, Israel	Boroda et al. (2011), Boroda et al. (2013)

originally generated through deflation, but subsequently developed a strong rock varnish coating and the Av horizon accumulated beneath the chert cobbles (Brookes, 1993).

Desert pavements formed by processes other than deflation appear to be polygenetic landforms, perhaps exhibiting equifinality, where different processes can act over time to generate a similar form. Table 2 compiles the variety of different factors and processes thought to promote the formation of non-deflation desert pavements. All of the factors presented in Table 2 are consistent with pavement cobbles that are coated with rock varnish (Dorn, 1986). Similarly, if aeolian activity was sufficient to winnow fines, the vesicular Av soil horizon of accumulated dust would not exist underneath pavement clasts. Within the last few decades, considerable research has focused on this dust accumulation (*e.g.* Table 3).

2.3. Constraining ages of desert pavements using different approaches

The growth of chronometric techniques in the past few decades has been vital to developing a better understanding of desert pavement longevity. Each employed technique provides a different chronometric perspective. For example, K-Ar or $^{40}Ar/^{39}Ar$ ages for a lava flow provide a maximum-limiting age for the pavement formed on top of the flow. Conversely, varnish microlamination (VML) dating provides insight into when the very surface of a pavement clast last experienced erosion and hence provides a minimum-limiting age for the pavement. Cosmogenic nuclides generate very different information – often a complex picture of the surface exposure history of pavement clasts. Table 4 presents a compilation of the array of different techniques that have been used to assign ages to desert pavements.

2.4. How long does it take to form a desert pavement?

Advances in dating techniques (Table 4) has resulted in new insight into how long it takes to go from a rough surface, such as the bar-and-swale deposits of a desert flood or a debris flow, to a smooth pavement surface. The length of time required to smooth a surface depends on a number of factors including: rock type and how the rock is jointed; the original size of the material; rates of aeolian deposition of fines; climate and paleoclimatic changes; percent clays; relief of the deposit; slope; availability of decay agents such as salts; biotic activity; and seismic shaking (Cooke and Warren, 1973; Mabbutt, 1979; Dixon, 1994; Haff, 2005; Dixon, 2009).

Given the large number of variables influencing the time it takes to develop a desert pavement, the considerable time range noted Table 5

Table 2
Factors promoting desert pavement formation in settings that do not experience aeolian deflation.

Factor promoting pavement formation	Summary and references
Low slope (flat surface)	A surface with very low relief and with a minimal gradient promotes pavement development (Ugolini et al., 2008).
no gullying	A complete lack of gullying or swales enhances pavement formation (Peel, 1960; Cooke, 1970; Huang et al., 2014).
Minimal bioturbation	Minimal bioturbation enhances pavement formation (Musick, 1975; Wood et al., 2005; Matmon et al., 2009; Pietrasiak et al., 2014).
Clast size reduction by mechanical fracturing	Broad recognition exists that breakdown of pavement clasts helps smooth an originally rough surface morphology created by debris flows or bar-and-swale flood deposits (Peterson, 1981; Amit et al., 1993; Al-Farraj, 2008; Matmon et al., 2009; Bockheim, 2010; deHaas et al., 2014)
Creep reducing surface relief	Creep is a classic process in the pavement literature smoothing surfaces, supported by recent research (Denny, 1965, 1967; Haff, 2005; Dietze and Kleber, 2012; Dietze et al., 2013).
Overland flow	The removal of fines by overland flow is supported as an important pavement-forming process by a diverse array of data including ^{10}Be accumulation, by direct observations, laboratory modeling, and field studies of clast alignment (Sharon, 1962; Abrahams et al., 1990; Abrahams and Parsons, 1991, 1994; Williams and Zimbelman, 1994; Wainwright et al., 1995, 1999; Dixon, 2009; Dietze et al., 2013; Rodriguez et al., 2013b).
Upward stone movement	Initial research in Australia (Jessup, 1951, 1960; Mabbutt, 1965; Fisher et al., 2014) and the Great Basin, USA (Springer, 1958) focused on wetting and drying generating upward stone movement; further support for this process comes from geoarchaeology observations in Ethiopia, (Aerts et al., 2010), upfreezing by periglacial processes (Fuchs et al., in press), and beetle foraging (Haff, 2014).
Dust accumulation (flotation) under clasts	Dust flotation emerged as a pavement-forming process in Australia (Mabbutt, 1977; Mabbutt, 1979), followed by scholarship in the USA (McFadden et al., 1986; McFadden et al., 1987), in the Negev Desert (Gerson and Amit, 1987), in Patagonia of Argentina (Sauer et al., 2007), and in the Libyan Desert (Adelsberger and Smith, 2009; Adelsberger et al., 2013; Cremaschi et al., 2014)

should not be surprising. Still, an appropriate generalization would be that "well developed" pavements typically initiated during the last glacial cycle or before in warm desert settings.

A complication in reading the global pavement literature on the time required to generate a pavement is the subjective use of terms like "smooth", "well packed", "well developed" or "mature" pavement. These and similar descriptive terms are rarely quantified or qualified. Although replicable metrics of pavement development exist (Amit and Gerson, 1986; Al-Farraj and Harvey, 2000), such information is rarely presented along with chronometric results. This is not a critique of those using descriptive terminology, but rather a simple recognition that some of the time variability in Table 5 could be due to the lack of a unified definition of what is a "well developed" pavement.

Yet another issue in trying to reconcile different times required to generate a pavement includes factors that disturb a pavement – either while it is developing or after it has formed – particularly by biotic agencies (Musick, 1975; Huckleberry, 1993, 1994; Quade, 2001; Wood et al., 2005; Matmon et al., 2009; Pietrasiak et al., 2014) followed by subsequent regeneration. One strategy to deal with these interruptions involves numerical modeling to illustrate a dynamic steady state (Pelletier et al., 2007). A second reconciliation approach is the hypothesis that bioturbation creates a permanent end to pavements. In this view, there are stable desert pavements ("abiotic landform evolution") and then the disturbed pavement that moves towards a "biological landform evolution" pathway; these pathways results in two different landform systems on alluvial fans in locations like the Mojave Desert where both of them are stable: a desert pavement zone and a shrub zone (Pietrasiak et al., 2014). This "fork in the road" hypothesis is consistent with mapping of vegetation and soil-geomorphic surface mosaics in the Mojave and Sonoran deserts, where abiotic pavements maintain very different leaching depths and soluble salt concentrations than biologically active areas (Musick, 1975; Wood et al., 2005). A third reconciliation strategy – used in our case study of stream terraces presented later in this paper – is to employ both long-lived cosmogenic nuclides like ^{10}Be and short-lived isotopes like ^{14}C. For example, bioturbation episodes in the last 20,000 years can be recorded by the decay of *in situ* ^{14}C when cobbles move beneath the surface.

2.5. Evidence for ancient pavements

Table 6 presents the first compilation of a burgeoning array of dating results indicating that desert pavements exist as stable landforms for very long periods of time. Our approach in deciding what research to include in Table 6 is not to be exclusionary. We do not feel it is appropriate to play the role of an international committee to judge which site is truly the "oldest desert pavement" on Earth.

Table 3
Research themes on the vesicular Av dust deposit underneath non-deflation pavements.

Research topic	Finding	References
Ecological influences	Av horizons are linked to arid ecoregion distribution and disturbed by root activity.	Turk and Graham (2011), Dietze et al. (2012)
Field experiments	Flat and elongated cobbles trap dust most efficiently.	Goosens (1995)
Ground penetrating radar	For older pavements, GPR provides a reconnaissance means of mapping clay content.	Meadows et al. (2006)
Hydraulic properties	Av horizons influence soil hydraulics.	Young et al. (2004), Meadows et al. (2008)
Infiltration capacity studies	Av horizons and pavements decrease infiltration capacities.	Wilcox et al. (1988), Abrahams and Parsons (1991), McDonald et al. (1996)
Nitrate studies	Nitrate pools in soils exist under desert pavements.	Graham et al. (2008)
Optically stimulated luminescence studies	Ongoing dust deposition results in pavement flotation on a millennial timescale.	Guralnik et al. (2011); Fuchs et al. (in press), Dietze et al. (2016)
Small scale mapping	Dust trapping depends on pavement fabric and texture.	Wood et al. (2002), Wood et al. (2005)
Vesicle formation	Av horizons develop from wetting and drying cycles and subsurface sealing, and they can be stabilized by clays, calcium carbonate, and iron films on mineral grains.	Springer (1958), Evenari et al. (1974), McFadden et al. (1986), McFadden (1988), Valentin (1994), Turk and Graham (2011), Dietze et al. (2012), Lebedeva et al. (in press)
X-ray tomography of vesicles	Pore size and pore number are inversely related in Av horizon peds.	Turk and Graham (2014)

Table 4
Techniques used to measure the age of desert pavements.

Dating Method	Information Obtained	Limitations	References
^{14}C dating of pedogenic carbonate rinds	Minimum age for the overlying pavement	Pedogenic carbonate is mostly an open system with newer mass moving into older deposits (Stadelman, 1994).	Reheis et al. (1992), McDonald et al. (2003), Larson et al. (2010).
Cosmogenic exposure ages using radionuclides in single cobbles	Exposure history of cobbles at the surface	Requires correction for prior inheritance using subsurface samples	Shepard et al. (1995), Siame et al. (1997), Ewing et al. (2006), Owen et al. (2011), Gray et al. (2014), Huang et al. (2014)
Cosmogenic depth profiles	Analysis of nuclides in clasts at varying depths beneath a desert pavement yields an age estimate for the pavement	Requires correction for surface erosion and correction for inheritance, or the accumulation of cosmogenic nuclides in a prior geomorphic setting	Van Der Woerd et al. (2006), Machette et al. (2008), Blisniuk et al. (2010), Jungers et al. (2013), Gray et al. (2014)
Cosmogenic exposure ages using radionuclides in amalgamated samples	Time of cobbles exposure at the surface	Assumes that each of the cobbles being combined have a similar exposure history, that can be corrected for prior exposure by using amalgamated samples collected from depth	Anders et al. (2005), Marchetti and Cerling (2005), Matmon et al. (2009), Guralnik et al. (2010), Fisher et al. (2014).
Cosmogenic exposure using a stable nuclide (^{3}He or ^{21}Ne)	The cumulative buildup of stable nuclides means that each measurement is a maximum age for emplacement of the clast in the pavement.	Correction for prior exposure history of a clast at depth assumes a similar exposure history to pavement clasts	Dunai et al. (2005), Marchetti and Cerling (2005), Oskin et al. (2007), Evenstar et al. (2009), Fenton and Pelletier (2013)
K-Ar or $^{40}Ar/^{39}Ar$ on lava flow	Maximum age for pavement formation	Time between flow solidification and pavement genesis can vary	Wells et al. (1985), Valentine and Harrington (2006), Valentine et al. (2006), Fenton and Niedermann (2014)
Optically stimulated luminescence (OSL)	maximum age for the overlying pavement	Along with thermal luminescence (TL) and infrared stimulated luminescence (IRSL), OSL requires great care in sampling and sample processing.	Sohn et al. (2007), Matmon et al. (2009), Armstrong et al. (2010), Guralnik et al. (2011), Huang et al. (2014), Fuchs et al. (in press), May et al. (2015), Dietze et al. (2016)
Rock luminescence dating	Provides an exposure for rocks on the surface in a desert pavement	Results can be complicated by multiple exposure and burial events for a rock surface	Sohbati et al. (2015)
Roughness variations with radar data	Provides a calibrated age	Requires numerical ages to calibrate surfaces and requires regional calibrations	Hetz et al. (2016)
Th^{230}-U^{234} dating of pedogenic carbonate rinds	Mininum age for the overlying pavement	Open-system nature of the pedogenic carbonate system provides challenges	Ku et al. (1979), Reheis et al. (1992), Peterson et al. (1995), Blisniuk et al. (2012), Wright et al. (2014)
Varnish microlamination (VML)	Provides both minimum age and paleoclimatic history experienced by the pavement	Method relies on regional calibrations using numerical ages and requires care in sampling	Liu and Broecker (2007, 2008a, 2008b), Liu et al. (2013), Liu and Broecker (2013)

Instead, our goal has been to include all examples we could find in prior scholarship of ages for desert pavements. For example, a case could be made that Dunai et al. (2005) do not date a desert pavement, but rather cobbles on a sediment surface and that ^{21}Ne ages of 9 to 37 Ma simply reflect cumulative time at or near the surface. Still, we felt it appropriate to include these data in Table 6, because images E and F in the associated GSA Data Repository item 2005053 would certainly qualify as a desert pavement if seen as a blind image by most researchers. Similarly, Appendix DR1 in the Data Repository 2009007 of Evenstar et al. (2009) shows a photograph of a surface that is explicitly described as a desert pavement "covered by clasts ranging in size from pebbles to boulders (~1 m)". Thus, while Evenstar et al. (2009) focused on ^{3}He ages as an indication of Cenozoic climatic change, the paper was included in Table 6 because the sampling context was clearly a desert pavement. Ewing et al. (2006) present ^{10}Be and ^{26}Al exposure times for surficial boulders of 2.12 ± 0.05 Ma with erosion rates of 0.160 ± 0.014 m/Ma, and we decided to include this paper, because Fig. 10 in Ewing et al. (2006) present a graphic of a desert pavement on top of the Yungay soil profile. Wang et al. (2015: 234) similarly present a graphic of a desert pavement in their model as well as images of a desert pavement at their site location.

Placzek et al. (2014: 1491), in contrast, have a narrower view of what is and what is not a desert pavement when they write "[site 4 in the Atacama Desert] is one of the few desert pavements observed in the Atacama …" A logical next step would be for Placzek et al. (2014) to undertake a critical analysis of the ancient pavement literature laid out in Table 6 and explain in detail their views over which sites are not real desert pavements and why they should be excluded from a compilation of ancient pavement ages.

However, given the basic definition that a desert pavement is a gravel surface one or two stones thick (Mabbutt, 1965; Cooke, 1970; Mabbutt, 1979), we consider it important to be inclusive in the compilation presented in Table 6. Basically, we take the position that if the authors identify a desert pavement or if we are able to see a photograph or a graphic indicative of a reasonably classic desert pavement, it is included in Table 6.

Table 6 similarly does not present a critical analysis evaluating the validity of the various chronometric claims, because the research cited often goes into detail on uncertainties associated with sampling and analysis. Rather, the purpose of this compilation of pavement antiquity rests in revealing the wide variety of methods used to place minimum and maximum ages on pavements. The results of these different methods present a clear and compelling case for the antiquity of desert pavements in a wide variety of global contexts.

3. Case study of the oldest known desert pavement in the Sonoran Desert, North America

3.1. Introduction to the case study

An impressive variety of techniques and results reveal that desert pavement surfaces can survive Earth's dynamic surficial processes for lengthy periods of time ranging from 10^3 to over 10^6 years (Table 6). Pavement scholarship typically presents only brief explanations for this stability. For example, in a title arguing that "[d]esert pavement-coated surfaces in extreme deserts present the longest-lived landforms on Earth", Matmon et al. (2009: 688) attributed this extreme geomorphic stability to the "combination of long-term hyperaridity, absence of vegetation and bioturbation, and the rapid reduction of original chert and carbonate clasts into a full-mosaic of pebble-size desert

Table 5
Time required to develop a desert pavement in thousands of years (ka).

Ages (ka)	Context of sample collection	Location	Dating Method	References
1.4–6.2	samples collected under desert pavements on beach ridges	Patagonia, Argentina	^{14}C dating shells	Sauer et al. (2007)
5–6	samples collected under an incipient pavement	Mojave Desert, USA	IRSL and ^{14}C pedogenic carbonate	McDonald et al. (2003), Cyr et al. (2010)
8.3	Samples collected under pavement developed on alluvial fan after regional desiccation	Southern Arabia	^{14}C dating organics	Pietsch and Kuhn (2012)
6.0 ± 1.0	Samples from rough pavement	Precordillerra, Argentina	^{10}Be surface exposure dating	Hedrick et al. (2013)
6–40	Samples from pavement with bar and swale topography are ~6 ka; samples from smooth pavements range in age from ~35–40 ka in	Anza Borrego, USA	^{10}Be in pavement cobbles and U-series on pedogenic carbonate	Blisniuk et al. (2012)
7	Samples collected from fill terrace alluvium underneath "weak pavement"	Grand Canyon, USA	OSL	Anders et al. (2005)
11.1 ± 4.3	Samples from pavement with subtle swale topography	Dead Sea, Near East	^{10}Be surface exposure dating	LeBeon et al. (2010)
11–25	Samples collected under poor to moderate pavement 11–17 ka and under well-developed pavements 25 ka	Death Valley, USA	OSL on alluvium under pavement	Sohn et al. (2007)
12–18	Samples from incipient pavements 12–18 ka, and samples from well developed pavements 24–128 ka	Death Valley, USA	Varnish microlaminations	Liu and Broecker (2008a, 2008b)
12	"Poorly packed" pavement occurs on alluvial fan surfaces <12 ka, while "moderately to well packed" pavements occur on surfaces with 12–30 ka ages	Death Valley, USA	^{36}Cl depth profiles	Machette et al. (2008)
13–25	Samples from pavement with relict bar-and-swale topography yield 13–15 ka ages, while mature smooth pavements yield ages older than 25 ka	southern Nevada, USA	Varnish microlaminations	Dickerson et al. (2013)
14	Samples from pavement with some bar and swale topography	Atacama Desert, northern Chile	^{10}Be surface exposure dating	Cortes et al. (2012)
15	Samples collected under a smooth pavement surface	southern Nevada, USA	^{14}C pedogenic carbonate	Reheis et al. (1992).
15.5 ± 2.2	Samples from a pavement that still retains some bar-and-swale topography	Baja California, Mexico	^{10}Be surface exposure dating	Spelz et al. (2008)
17–35.5	Samples from a weakly developed Desert pavement	Coachella Valley, USA	^{10}Be surface exposure dating	Gray et al. (2014)
35.5 ± 2.5	Samples from a well-developed pavement with only subtle expressions of bar-and-swale topography	Coachella Valley, USA	^{10}Be surface exposure dating	Van Der Woerd et al. (2006)
56.4 ± 7.7	Samples from patchy and weakly-developed pavements with patches of interlocked pavement	Mojave Desert, USA	^{10}Be surface exposure dating	Oskin et al. (2007)
58–67	Well developed and "flat-surfaced" pavement formed sometime after an OSL age of ~58 ka; while the ^{10}Be exposure age is 66.6 ± 6.8 ka after correcting for inheritance	Tian Shan, China	^{10}Be surface exposure dating and OSL on alluvium under pavement	Huang et al. (2014)
70	Desert pavement goes through a transition from prominent bar-and-swale topography, immature pavement, moderate pavement, and then mature pavement, and this entire transition requires ~70 ka	Death Valley, USA	^{10}Be exposure dating and ^{36}Cl depth profiles	Frankel and Dolan (2007)
100 ± 22	Samples from a "poorly developed" desert pavement	Precordillera, Argentina	^{10}Be surface exposure dating	Siame et al. (1997)

pavement." While Matmon et al. (2009) make a compelling case for their hyperarid Middle Eastern setting, our point is that research into explanations for pavement stability must include more than hyperarid conditions and should encompass ancient desert pavements around the globe whose antiquity cannot be explained by these factors alone.

This case study focuses on the Sonoran Desert, North America, in part because it is not hyperarid and can experience bioturbation. Annual precipitation averages 208 mm and is evenly divided between winter and monsoon maxima. Winter rainfall comes from Pacific low-pressure systems. Summer rainfall derives from summer thunderstorms during the July–September monsoon season where air masses come from the Gulfs of Mexico and California. Aeolian activity consists of dust storms associated with downburst winds. Very little evidence of aeolian abrasion exists in the Sonoran Desert outside dune fields such as the Cactus Plains wilderness or the Gran Desierto de Altar. The general aridity of the Sonoran Desert and the abundant dust deposition both contribute to the stability of desert pavements in this desert.

This case study focuses on the discovery of the oldest known desert pavement in the Sonoran Desert at ~332 ± 4 ka; we evaluate this pavement survived for 10^5 years, whereas pavements on older nearby landforms did not. Then, after this case study, we conclude this paper by reanalyzing factors that contribute to pavement longevity, and conversely, factors that contribute to the desert pavement instability.

3.2. Study site: Desert pavements on Salt and Verde Terraces, central Arizona, USA

Strath and fill terraces of the Salt and Verde Rivers (Pope, 1974; Péwé, 1978; Skotnicki et al., 2003; Cook et al., 2010; Larson et al., 2010) offer a setting to understand the longevity of desert pavements. Located in the north-central Sonoran Desert (Fig. 2), near Phoenix, Arizona, USA flights of terraces offer a range of landforms in a classic relative age sequence (Figs. 3, 4a, b). A relative sequence of oldest terrace (highest) to youngest terrace (lowest) offers an independent check on numerical ages for desert pavements formed on terrace treads.

Prior research on the ages of these terraces provided only minimal chronometric information: (1) a minimum age for the Blue Point terrace of the Salt River of 33,100 ± 380 calendar years, based on radiocarbon dating of an innermost carbonate rind with a laminar texture around gravel in the Bk horizon underneath the desert pavement (Larson et al., 2010); and (2) a single unpublished preliminary ^{36}Cl surface exposure age of ~440 ka for amalgamated pavement cobbles collected from the Salt River's Mesa terrace (Campbell, 1999) using unknown production rates. Thus, to improve the quality and the quantity of age control on pavements atop the stream terraces, we employed cosmogenic ^{10}Be, ^{14}C, and ^{26}Al dating strategies to better understand the ages of desert pavements on this terrace sequence.

Table 6
Reported ages of desert pavement around the globe, ordered from oldest to youngest.

Age	Region	Method	References	Notes	Landform host
9–37 Ma	Atacama, Northern Chile	^{21}Ne	Dunai et al. (2005)	Measurements from quartz clasts in desert pavements indurated by carbonate and salts	Alluvium
1.2–22 Ma	Atacama, Northern Chile	^{3}He	Evenstar et al. (2009)	Measurements from larger basalt clasts in pavement indurated with gypsum	Pediplain
3.9–15.15 Ma	Victoria Land, Antarctica	^{40}Ar/^{39}Ar and K/Ar	Marchant et al. (1993), Marchant and Denton (1996), Marchant et al. (1996)	Dated ash overlies stone pavement was determined.	Buried glacial deposits
3.7 ka — 15 Ma	Transantarctic Mountain, Antarctica	Dating of the underlying landform in cited prior research	Bockheim (2010)	Ventifaction increases while clast sizes decreases over time	Glacial deposits
9 Ma	Atacama Desert, Chile	^{10}Be, ^{26}Al, ^{21}Ne	Nishiizumi et al. (2005)	Sampled from quartzite cobble in pavement composed of angular clasts	Alluvial fan
6.6 Ma	Atacama Desert, Central Valley, Chile	Meteoric ^{10}Be in soil profile collected at 5 cm intervals	Wang et al. (2015)	Ventifacted pavement cobbles indurated with gypsum caps analyzed soil profile	Alluvial fan
>3 Ma	Atacama Desert, Chile	^{10}Be	Placzek et al. (2014)	Corrected for inheritance and analyzes the influence of minor erosion.	Stable alluvial surface
2–4 Ma	South-Central Australia "stony deserts"	^{21}Ne, ^{10}Be	Fujioka et al. (2005)	Cobbles composed of gibber (silcrete cobbles)	Alluvial fan; tablelands
2.12 Ma	Atacama, Central Chile	^{10}Be, ^{26}Al	Ewing et al. (2006)	Desert pavement at Yungay site with minimal evidence of ventifaction sampled in pavement indurated with salts	Alluvium
260 ka–1. 8 Ma	Dead Sea region, Middle East	^{10}Be, OSL	Matmon et al. (2009), Guralnik et al. (2010)	Stone pavement on alluvium, with amalgamation sampling	Alluvial terraces and deposits
0.9–1.8 Ma	Fowlers Gap, New South Wales, Australia	^{10}Be, ^{26}Al	Fisher et al. (2014)	Stone pavement on alluvial surface; amalgamation sampling	Pediment
~0.25–1.5 Ma	Atacama Desert, Chile	^{10}Be, ^{26}Al	Amundson et al. (2012), Jungers et al. (2013)	Pavements developed on landforms after abandonment	Alluvial fan and fill terrace
0.3–1.12 Ma	Negev Desert Israel	^{10}Be assuming clasts remained at the surface; maximum age for pavement	Boroda et al. (2014)	Amalgamation simple exposure age considered minimum age for pavement	Top of bedrock mesa
1.1 Ma	North-central Chile	^{10}Be	Rodriguez et al. (2013a)	Slow removal of fines blends longer-exposed cobbles with more newly-exposed cobbles	Fluvial terrace
119 ka–1 Ma	Atacama Desert, Chile and Peru	^{10}Be	Hall et al. (2008)	Sampled cobbles derive from desert pavements	Pediments and strath fluvial terraces
77 ka–1 Ma	Basin and Range, Crater Flat, Southern Nevada, USA	^{40}Ar/^{39}Ar, ^{36}Cl and K/Ar	Zreda et al. (1993), Heizler et al. (1999), Valentine and Harrington (2006), Valentine et al. (2006)	Silt accumulation underneath lapilli in a particular size range produces stable pavements	Basalt flow
17 ≤ 730 ka	Great Basin, Crater Flat, Nevada, USA	Th^{230}-U^{234} dating of pedogenic carbonate under pavement; and CR dating	Peterson et al. (1995)	Stone pavements on different geomorphic surfaces	Alluvial fan units and basalt flows
41–670 ka	Iglesia basin, central Andes, Argentina	^{10}Be	Siame et al. (1997)	Mixture of ^{10}Be ages implies mixing of cobbles with different exposures through deflation and periglacial processes	Alluvial fan
49–610 ka	Negev Desert, Israel	^{10}Be	Boroda et al. (2011), Boroda et al. (2013)	Pebble sized chert desert pavement clasts	Talus flatiron
224–600 ka	Great Basin, Lunar Crater, Nevada, USA	^{36}Cl	Shepard et al. (1995)	Boulders (10–15 cm) in stone pavement formed on the lava flow bedrock	Basalt flow
32–~580 ka	Cima Volcanic Field, Mojave Desert	^{3}He, OSL, K-Ar of underlying basalt flows	Turrin et al. (1985), Wells et al. (1985), McFadden et al. (1987), McFadden et al. (1998), Dietze et al. (2016)	Pavements develop through accumulation of aeolian dust under clasts	Basalt flow
260–505 ka	Bishop Tuff, California, USA	^{21}Ne	Goethals et al. (2007)	Pavement samples show less age variation than bedrock samples	Welded tuff
57–428 ka	Tian Shan, China	^{10}Be, OSL	Huang et al. (2014)	Minimal erosion occurs on pavements younger than 428 ka	Strath fluvial terraces
424 ± 151 ka	Atacama Desert, northern Chile	^{21}Ne	Gonzalez et al. (2006)	Pavements on fans abandoned by faulting	Alluvial fan
420 ± 16 ka	Gobi-Altai Mountains piedmont	^{10}Be	Lv et al. (2010)	Age based on assumption of low inheritance	Sloping alluvial plain
281 ± 19 ka	Lanzarote, Canary Islands	^{40}Ar/^{39}Ar; ^{3}He	Dunai and Wijbrans (2000)	Lava flow blocks in the desert pavement sampled for both dating methods	Basalt flow
3–280 ka	Mecca Hills, Colorado Desert, USA	^{10}Be surface exposure and depth profiles	Gray et al. (2014)	Stone pavement development with occasional boulders sampled for ^{10}Be	Alluvial fan units

Table 6 (*continued*)

Age	Region	Method	References	Notes	Landform host
<12 ka, 50–100 ka, 130 ka, 150 ka, > 260 ka	Great Basin, Death Valley, California, USA	^{10}Be, ^{26}Al, ^{36}Cl: depth profile and on surface clasts	(Nishiizumi et al. (1993), Duhnforth et al. (2007), Frankel et al. (2007a, 2007b), Machette et al. (2008), Owen et al. (2011), Ivy-Ochs et al. (2013)	Stone pavements on different surfaces, where inheritance of different sized clasts creates ambiguities in ages	Alluvial fan units and Lake Manly shorelines
<63 ka to <350 ka	Lower Colorado River, USA	^{3}He	Fenton and Pelletier (2013)	Basalt boulders on desert pavements	Alluvial fan
12–245 ka	Death Valley, California	Varnish microlaminations	Liu and Broecker (2008b)	VML records minimum age for exposure of the sampled pavement clast	Alluvial fan
204 ± 11 ka and older (based on stratigraphy)	Laguna Salada, Baja California, Mexico	^{10}Be	Spelz et al. (2008)	Incipient pavement on Q_6 and well-developed pavements found on Q_7 (204 ± 11 ka) and Q_8	Alluvial fan
66–198 ka	West Grand Canyon, USA	^{3}He,	Fenton et al. (2002), Fenton et al. (2004)	Pavement on basaltic outburst flood deposit	Stream terrace
141–184	South Sheba lava flow, San Francisco volcanic field, Colorado Plateau, Arizona, USA	^{3}He, ^{21}Ne,	Fenton and Niedermann (2014)	Two pavements have similar ages to pressure ridges	Pavement formed on basalt flow
24–181	Eastern Precordillera, Argentina	^{10}Be	Hedrick et al. (2013)	Well-developed pavements are more stable for longer periods on strath (up to ~181 ka) terraces than fans (up to ~61 ka)	Strath stream terrace and alluvial fans
170 ka	Negev Desert, Israel	^{10}Be, OSL	Guralnik et al. (2011)	Pavement formed after terrace abandonment with stability enhanced by gypsum	Fill stream terrace
97–159 ka	Capitol Reef, Utah, USA	^{3}He	Marchetti and Cerling (2005)	Dated by amalgamation, pavements are 34–96 ka younger than boulder exposure ages	Fill stream terrace composed of debris-flow deposits
137 ± 9 ka	Northeast Tibet	^{10}Be, ^{26}Al	Shirahama et al. (2015)	Pavement consists of pebbles	Strath terrace
31–132 ka	Northwest Argentina	^{10}Be	Siame et al. (2015)	Pavements have dark rock varnish	Strath terraces
100–130 ka	Lake Eyre, Australia	Soil and pavement stratigraphy	Al-Farraj (2008)	Pavement with varying stone cover	Beach gravel
15–130 ka	Kyle Canyon, southern Nevada, USA	^{14}C, Th^{230}-U^{234}	Reheis et al. (1992)	Secondary carbonate dated from soil positions	Alluvial fan
7–109 ka	Tributaries of the Grand Canyon, USA	^{10}Be, OSL	Anders et al. (2005)	OSL on terraces up to 50 ka; amalgamation sampling of pavement clasts for ^{10}Be	Fill stream terraces
106 ± 15 ka	Gonghe basin, Tibet	^{10}Be	Perrineau et al. (2011)	Larger pavement cobbles sampled	Strath terrace
106 ka	Chocolate Mountains, Colorado Desert, USA	Th^{230}-U^{234} dating of pedogenic carbonate under well-developed pavement	Wright et al. (2014)	Pedogenic carbonate on "Q3" surface provides minimum age	Alluvial fan
100 ka	Libyan Plateau, Egypt	Archaeological evidence: Middle Paleolithic artifacts in pavement	Adelsberger and Smith (2009)	Pavement on regolith	Bedrock plateau
70–96 ka	Vidal Valley, Mojave Desert, USA	Th^{230}-U^{234} dating of pedogenic carbonate under well-developed pavement	Ku et al. (1979)	Pedogenic carbonate on "Q2b" surface provides minimum age	Alluvial fan
90 ka	Qilian Shan, Northern Tibet	^{10}Be, ^{26}Al	Hetzel et al. (2004)	Clasts sampled from fluvial terrace where pavement inferred from descriptions	Alluvial fan
13–87	Great Basin, Stonewall Flat, Nevada	Varnish microlaminations and ^{10}Be	Dickerson et al. (2013, Dickerson and Cocks (2015)	Sampled away from evidence of bioturbation	Alluvial fan
11–87	Dead Sea, Israel	^{10}Be	LeBeon et al. (2010)	Pavement clasts sampled on deposits offset by faulting	Alluvial fan
84 ka	Lees Ferry, Colorado Plateau, USA	OSL and ^{10}Be	Hidy et al. (2010)	Pavement on Colorado River gravels	Fill river terrace
44–84 ka	Tashkurgan Valley, Xinjiang Province, China	^{10}Be	Owen et al. (2012)	Age range on Tashkurgan stage boulders in a desert pavement	Moraine
51–82 ka	Badia Jordan	OSL	Fuchs et al. (in press)	OSL samples from aeolian silt and sand underneath pavements	Basalt lava flow
71–72 ka	Fremont River and Wind River, Rocky Mountains, USA	^{10}Be, ^{26}Al	Anderson et al. (1996)	Cobbles samples from pavement on glacial outwash terrace, corrected for inheritance	Strath river terrace
40–60 ka	Chajnantor Plateau, Chile	^{10}Be, ^{36}Cl	Ward et al. (2015)	Sampled clasts from desert pavements	Moraines
56.4 ± 7.47 ka	Mojave Desert, USA	^{3}He, ^{10}Be	Oskin et al. (2007)	Pavement clasts collected with amalgamation strategy and considering inheritance	Alluvial fan, offset by faulting
5–56 ka	Providence Mountains, Mojave Desert, USA	^{10}Be, OSL, IRSL, ^{14}C on carbonate	McDonald et al. (2003), Cyr et al. (2010)	Incipient pavements require ~ 5–6 ka to form	Alluvial fan
~25–50 ka	Mojave Desert, USA	^{14}C	Meek (1989, 1990, 2004), Reheis and Edwine (2008)	Pavement consists of rounded cobbles on top of dated shells	Beach ridge and shorelines

(*continued on next page*)

Table 6 (*continued*)

Age	Region	Method	References	Notes	Landform host
5–47 ka	Anza Borrego, Colorado Desert, USA	^{10}Be: surface and depth profiles; Th^{230}-U^{234} dating of pedogenic carbonate	Blisniuk et al. (2012)	^{10}Be and U-series ages are consistent	Alluvial fan
44 ka	South Iran	^{10}Be	Regard et al. (2006)	Quartzite gravels sampled from desert pavement	Alluvial-fan gravels on anticline
35 ± 7 ka, 35 ± 2.5 ka	Coachella Valley, Colorado Desert, *CA*, USA	^{10}Be: surface and depth profiles	VanDerWoerd et al. (2006), Blisniuk et al. (2010)	Pavement on fan units offset in San Jacinto and San Andreas Fault Zones	Alluvial fan gravels
14–35 ka	Northern Chile	^{10}Be, OSL	Cortes et al. (2012)1	Minor and swale topography remains on younger 14 ka pavement	Alluvial fan, offset by faulting
33 ± 0.4 ka	Salt River, central Arizona, USA	^{14}C	Larson et al. (2010)	Pedogenic carbonate, innermost rind yields minimum age for the overlying pavement	Strath terrace
33 ka	Lake Frome, southern Australia	OSL	May et al. (2015)	Pavement on dated aeolian dust covering gravels	Beach ridge
17–30 ka	Sierra El Mayor, Baja California, Mexico	^{10}Be, OSL	Armstrong et al. (2010)	Smooth pavement with varnished quartzite and schistose cobbles tops terrace treads	Stepped strath terraces
11–25 ka	Great Basin, southern Death Valley, USA	OSL	Sohn et al. (2007)	Poor to moderate pavement formation takes 11–17 ka, but well-developed pavements occur in 25 ka	Alluvial fan
24 ka	Mojave River, Mojave Desert, *CA* USA	OSL, ^{10}Be	Cyr et al. (2015)	Pavement age represents the most recent cobble transportation event along the Mojave River	Strath terrace
3–20 ka	Andean Precordillera, Argentina	^{14}C, ^{10}Be pebble amalgamation	Schmidt et al. (2011)	Holocene terraces have poor pavement development compared to Pleistocene terraces	Strath terrace
11.1–12.34	Owens Valley, California, USA	Varnish microlaminations	Mihir et al. (2015)	Minimum age for debris flow fans	Debris flow deposits

We sampled four terraces along the Salt River and two terraces along the Verde River for study (Fig. 4). Fig. 5 shows oblique aerial views of the terraces with desert pavements analyzed with ^{10}Be, while Figs. 6 and 7 present 3 views of each sampling site: a ground view of the sampled desert pavement; a close-up showing the shape and dimensions of the sampled quartzite cobbles; and a cross-sectional perspective of the pavement and geological material underlying the terrace gravels.

3.3. Methods

3.3.1. Cosmogenic ^{10}Be, ^{14}C analysis of pavement clasts

3.3.1.1. Sampling

Research on the pediment systems of the region previously presented ^{10}Be data for desert pavement cobbles on the Blue Point and Mesa terraces (Fig. 4; Fig. 6A–F) of the Salt River (Larson et al., 2017). This case study greatly enlarges the data set on cosmogenic ^{10}Be and ^{14}C analyses for these and cobbles on four other stream terraces: Sawik and Stewart Mountain terraces of the Salt River; and Mesa and Lousley Hills terraces of the Verde River (Fig. 4; Figs. 6G–L; 7).

An ongoing literature discussion exists on the best types of samples to collect from desert pavements in order to constrain the age of the underlying landform. Strategies include collecting the largest boulders, collecting pebbles in different size fractions, collecting amalgamated samples, collecting depth profiles, and using different cosmogenic nuclides (Zimmerman et al., 1994; Anderson et al., 1996; Heimsath et al., 2001; Fujioka et al., 2005; Frankel et al., 2007a; Blisniuk et al., 2010; Owen et al., 2011; Jungers et al., 2013; Boroda et al., 2014; Gray et al., 2014).

The approach utilized here for stream terraces with a flat topography covered by desert pavement starts with the collection of individual quartzite clasts on the surface of desert pavements (Figs. 6–7). Field observations reveal that dust is trapped efficiently underneath pavement cobbles with this flattened shape (Goosens, 1995). Following prior scholarship that dust flotation helps maintain pavements collected clasts have a disk shape such that a flat surface rests on the Av horizon

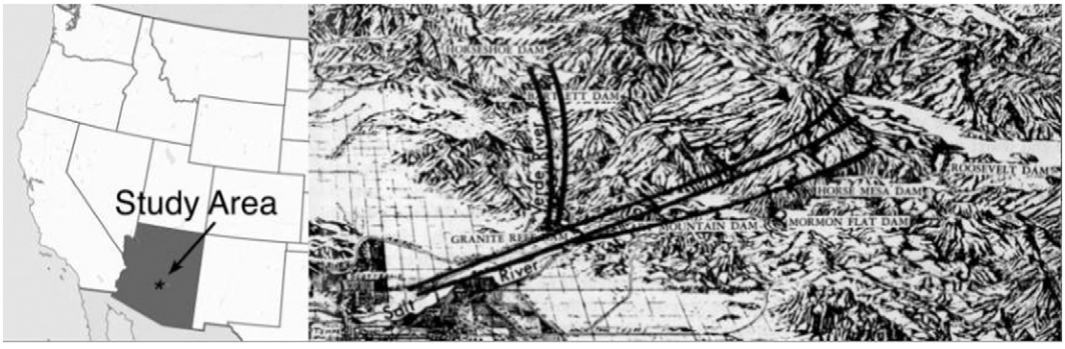

Fig. 2. Salt River Project's physiographic diagram served as the basemap for identifying the setting of strath terraces along the Salt and Verde Rivers (Péwé, 1978). Metropolitan Phoenix occurs in the lower left corner of this diagram.

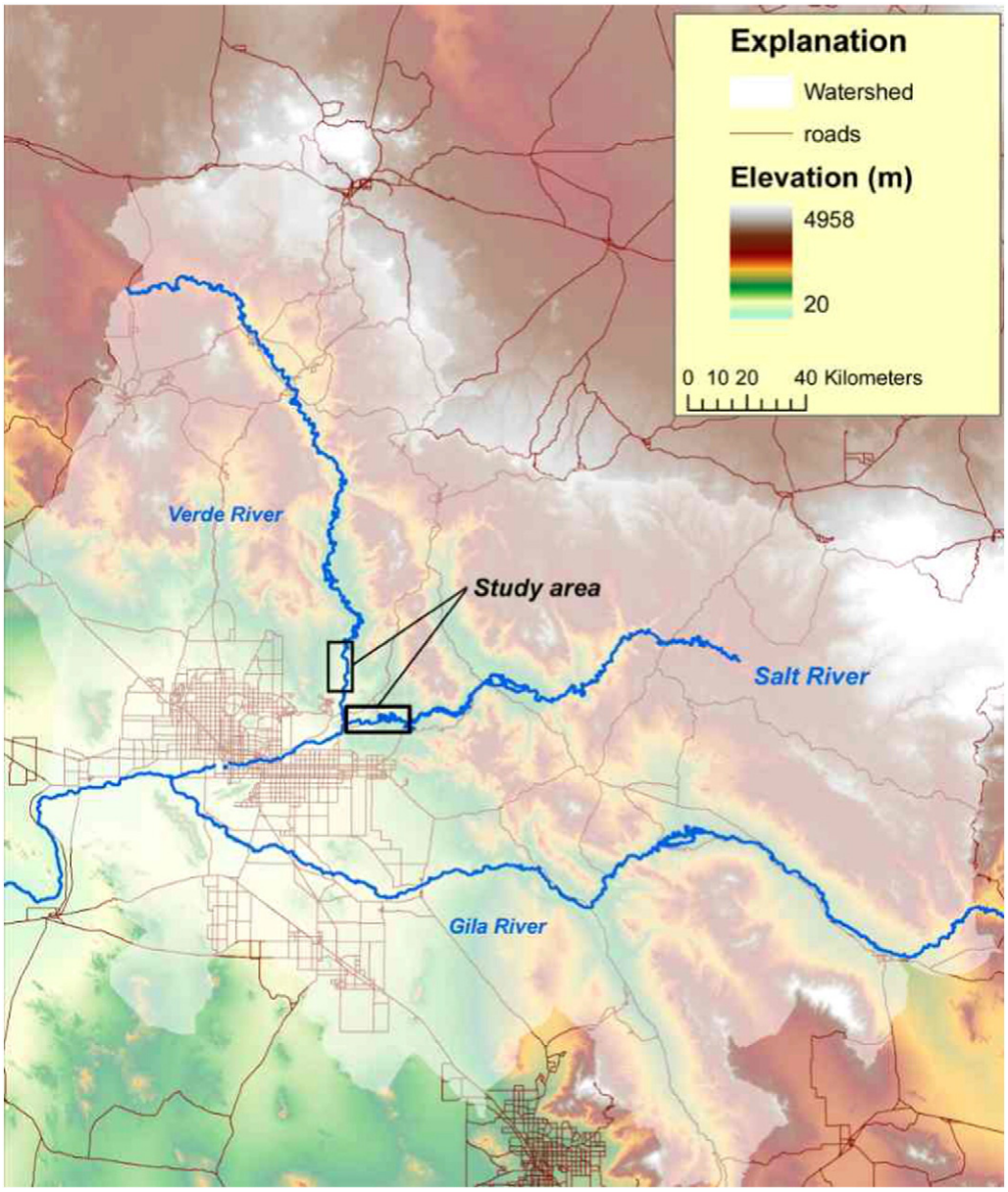

Fig. 3. Stream terraces along the lower Salt and Verde rivers, northeast of metropolitan Phoenix, offer a range of landforms ages capped by desert pavements. Fig. 4 presents the sequences of terraces observed in profiles across the middle of the identified study areas.

that has its origin in dust (see Section 2.2). The collected clasts also retain the original fluvially-abraded texture of smooth rounded edges. Thus our working hypothesis while in the field was that these quartzite disks have remained exposed to cosmic rays since their initial abandonment, floated by allochthonous aeolian dust input. Two sites, however, did not display an Av horizon indicative of a dust origin: Stewart and Lousley Hill pavements.

In situ accumulation of ^{14}C in quartz offers a test of the hypothesis that pavement cobbles have remained at the surface for the last ~20 ka. Because of the much shorter half-life of ^{14}C, burial by aeolian deposits or by bioturbated fines deposited on top of pavements would result in greater decay of ^{14}C than ^{10}Be (Lal, 1991). In contrast, a lower ratio of $^{10}Be/^{14}C$ results from continuous exposure on the surface. Thus, *in situ* ^{14}C was measured in some of the same cobbles analyzed for *in situ* ^{10}Be in the Sawik terrace pavement.

Older and higher alluvial surfaces often do not retain a flat topography with extensive desert pavements (Frankel and Dolan, 2007; Hedrick et al., 2013). This is the case for the Stewart Mountain (Fig. 5F) and Lousley Hills (Fig. 5D) terraces. While patches of pavements extensively cover the surface of these terraces (Figs. 6J, 7D), the lack of an Av horizon (and sand instead) could potentially reflect an origin derived through erosion of the terrace fill.

Assessment of the prior exposure history utilized roadcuts of over 5 m expose cross-sections at two of the terrace sites (Mesa Salt, Mesa Blue Point), and natural gullies expose cross-sections of over 3 m that were cleaned up prior to sampling. An amalgamation strategy involved collection of >30 quartz-rich cobble clasts buried with over 3 m of shielding to evaluate the prior exposure history. A pair of $^{10}Be/^{26}Al$ analysis for the buried amalgamation sample taken from the Sawik terrace was accomplished to constrain the burial age of the terrace (Granger, 2006).

3.3.1.2. Treatment and analysis

All samples were treated in the Cosmogenic Nuclides Laboratory of Korea University, following the standard method (Kohl and Nishiizumi, 1992). Crushed samples were sieved to the 250–500 μm

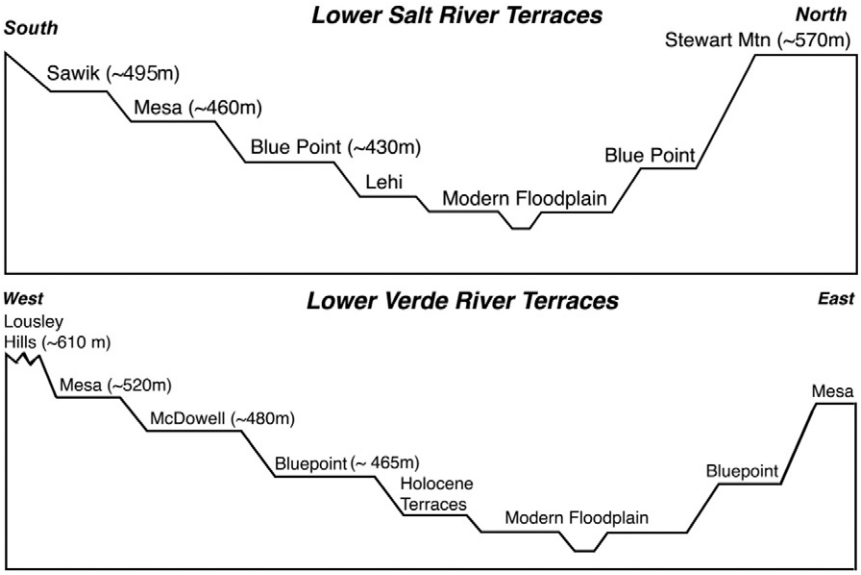

Fig. 4. Stream terraces along the lower Salt and Verde rivers, northeast of metropolitan Phoenix, where these idealized profiles represent sequences in the middle of the study areas identified in Fig. 3. The exact sampling locations are provided with the data (Table 7).

fraction and then treated typically with HF-HNO_3 to remove meteoric beryllium and organic matter. ~400 μg of low (<10^{-15} in $^{10/9}$Be) resolution ^{9}Be carrier is added and then Be and Al is separated by ion exchange and precipitated at pH > 7. Beryllium and Aluminum hydroxides are dried and oxidized at 800 °C for 10 min by ignition in a quartz crucible. BeO is then mixed with Nb and loaded into targets. They were measured

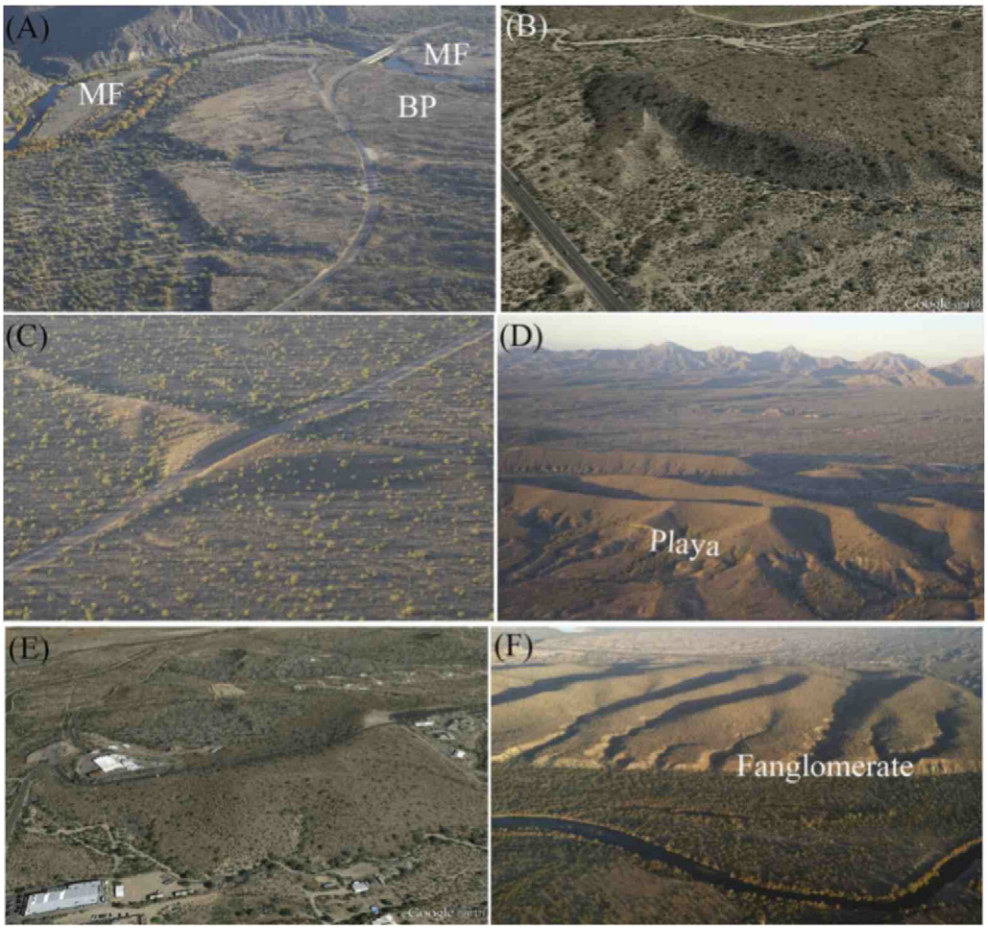

Fig. 5. Oblique aerial views of the Salt River (A-Blue Point, B-Mesa, C-Sawik, F-Stewart Mountain) and Verde River (B-Mesa, D-Lousley Hills) terraces sampled for ^{10}Be. The Lousley Hills (D) and Stewart Mountain (F) are fill terraces and are heavily incised by deep gullies, while the other terraces exist as isolated remnants. In image A, BP and MF identify the Blue Point strath terrace and modern floodplain. Roads provide a sense of scale in A–C and E. The 110 m difference between the Salt River's floodplain and the top of the Stewart Mountain terrace in F, and the 50 m thickness of the gravels in the Lousley Hills gravels above underlying playa sediment in D provide a sense of scale. Images B and E are from Google Earth, while the others imagery taken from an airplane.

Fig. 6. Sampling sites for ^{10}Be in the Salt River terraces (A–C Blue Point, D–F Mesa, G–I Sawik, J–L Stewart Mountain). Individuals and 0.5 m high creosote bushes (*Larrea tridentada*) provide a sense of scale for the desert pavement views (A D, G, J). Rock hammers indicate scale for the sampled disk-shaped cobbles (B, E, H, K). Images C, F, and I show granitic material forming straths underneath the Blue Point, Mesa and Sawik terraces, while a 45 m stream cut shows the fanglomerate base underneath approximately 30–40 m of fill atop the Stewart Mountain (L) terrace.

using 6MV Accelerator Mass Spectrometry (AMS) at the Korea Institute of Science and Technology (KIST), Seoul, Korea (Kim et al., 2016).

After blank (3×10^{-15} $^{10/9}$Be) correction and normalization of isotope ratios to ^{10}Be standards (Nishiizumi et al., 2007) using a ^{10}Be half-life of 1.387 ($\pm$0.03) $\times$ 10^6 yr (Chmeleff et al., 2010; Korschinek et al., 2010) we converted measured ratios into an absolute ratio of ^{10}Be/^{9}Be in quartz. Inheritance produced during prior exposure was quantified from amalgamated cobbles ($n > 30$) obtained from deep (>5 m) location and corrected for surface samples. We calculated ^{10}Be exposure ages using the CRNOUS exposure age calculator version 2.2 (Balco et al., 2008) by integrating shielding conditions, latitude-altitude production rate-functions (Lal, 1991; Stone, 2000; Heisinger et al., 2002a; Heisinger et al., 2002b) applying 4.49 $\pm$ 0.39 g^{-1} y^{-1} at SLHL (sea-level, high-latitude) for the ^{10}Be reference spallation production rate in this study (Stone, 2000; Balco et al., 2008). In addition, we also yielded ^{10}Be exposure ages applying local production rate of North America recently reported for comparison using a spallogenic production rate of 4.33 $\pm$ 0.21 g^{-1} y^{-1} at SLHL (Balco et al., 2009). The difference between global and regional production rates causes 3.58–3.89% in ages but we used the ages calculated using global production rate for the easiness of comparison with the previous studies. Propagated errors in the model ages include a 6% uncertainty in the production rate of ^{10}Be and a 4% uncertainty in the ^{10}Be decay constant.

Some of samples that were analyzed for ^{10}Be were also analyzed for *in situ* ^{14}C. The quartz cleaned in the Cosmogenic Nuclide Laboratory of Korea University were analyzed in the chemical lines modified from the previous *in situ* ^{14}C extraction systems (Lifton et al., 2001; Naysmith, 2007; Hippe et al., 2009; Pigati et al., 2010; Hippe et al., 2013; Goehring et al., 2014; Kim et al., 2016). Approximately 5 g of clean quartz was loaded with melting flux ($LiBO_2$) in an alumina (Al_2O_3) boat that had been pre-melted in high-vacuum conditions and then preheated with a step-wise increase of temperature, at 500 °C for 1.5 h and at 750 °C for 1.5 h, to remove atmospheric ^{14}C contamination. *In situ* ^{14}C trapped in the quartz lattice was degassed and oxidized at 1100 °C for 3 h with ultrahigh-purity O_2, followed by subsequent cleaning steps with secondary oxidation in a quartz-bead combustion furnace and a cryogenic coil trap (Lifton et al., 2001; Naysmith, 2007; Pigati et al., 2010). The purified CO_2 was graphitized and then loaded into targets. The targets were also analyzed by AMS at KIST. The measured ratios were normalized to NIST oxalic acid (^{14}C/^{12}C: 134 pMC, $\delta^{13}C = -17.8‰$) and converted to ^{14}C

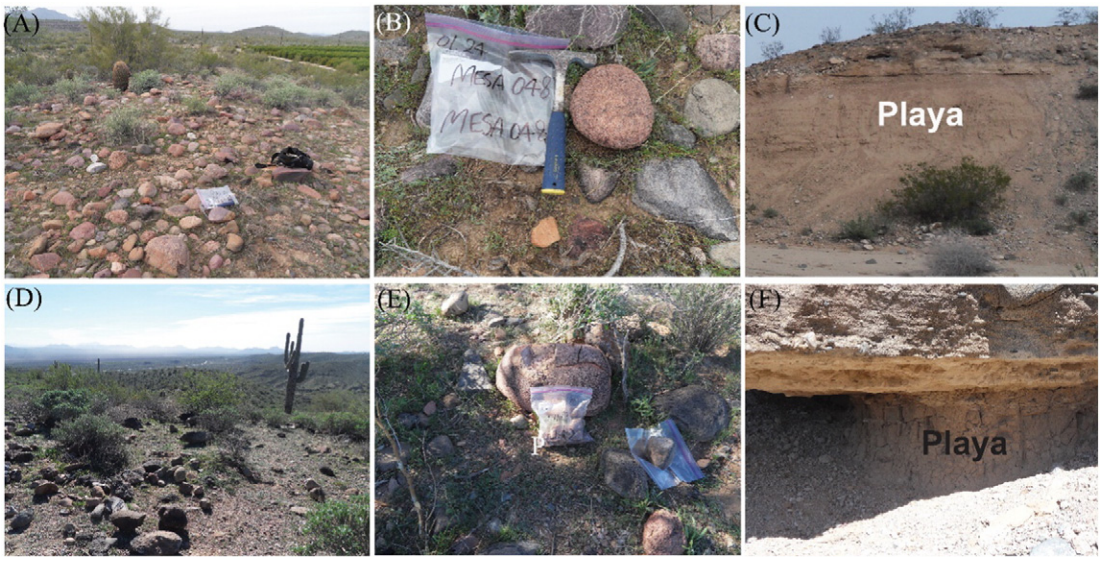

Fig. 7. Sampling sites for the Verde River sampled for ^{10}Be (A–C Mesa, D–F Lousley Hills). 0.5 m high brittlebush (*Encelia farinosa*) provides a sense of scale in the middle of the desert pavement views (A, D). Rock hammers indicate scale for the sampled disk-shaped cobbles (B, E) size and disk-shape. Image C highlights playa clays forming the strath that underlies ~3 m of Mesa Verde terrace gravels, and image F presents the basal contact of the Lousley Hills gravels on top of the same playa clays, where the vertical thickness in this view is about 0.6 m.

concentrations after correcting for blank readings (mean of $(5.99 \pm 2.58) \times 10^5$; n = 3).

3.3.2. OSL dating of the Blue Point Salt River terrace

OSL samples from the Blue Point terrace of the Salt River (Fig. 5A) were collected from the same study site as the prior study on carbonate rind radiocarbon dating (Larson et al., 2010). This is a strath terrace where bedrock granite is overlain by approximately 3–6 m of sediment (Fig. 6C). This alluvium is mostly gravel, but there are sandy lenses, and these were where the OSL samples were collected. Desert pavement cobbles of quartzite were collected for ^{10}Be analysis at the surface a few meters away from this OSL sampling location (Fig. 6A–B).

The samples were obtained by driving a stainless pipe, 25 cm in length and 7 cm in diameter, into the freshly exposed sand walls of the profile. The end of the pipe was quickly capped with aluminum foil upon retrieval, and the sample stored in a dark container. The samples were prepared and analyzed at the Korea Basic Science Institute (KBSI), Ochang, Korea using the single-aliquot regenerative-dose (SAR) protocol (Murray and Wintle, 2000). The SAR protocol for the optical measurements of quartz results in improved precision and accuracy for age determinations (Murray and Wintle, 2000; Murray and Olley, 2002). In the laboratory, samples were wet sieved to recover the 90–250 μm size fractions, and cleaned in 10% H_2O_2, 10% HCl, etched with concentrated HF, and the separated grains were pretreated for the preparation method of the SAR protocol of KBSI (Choi et al., 2003). All OSL measurements were performed using an automated Risø TL/OSL measurement system. Error is yielded based on saturated water contents.

3.3.3. Soil profile and rock varnish microlaminations

Standard USA Department of Agriculture guidelines were used to describe soil profiles (SoilSurveyStaff, 1974). Development of calcium carbonate horizons uses the desert soil project monograph stage classifications (Gile et al., 1981). The second author only provided field assistance in the previously unpublished soil profile analysis conducted by Troy Péwé (now deceased).

We also employed varnish microlaminations (VML) dating using established collection and calibration procedures (Liu and Broecker, 2008b, 2013; Liu, 2016). Ten samples for VML were collected from the Blue Point, Mesa, and Sawik terraces of the Salt River from the same pavements sampled for ^{10}Be dating. Since VML can only provide the age sequence of varnishes exposed at the surface, any bioturbation or cobbles spalling event would reset the VML clock; hence VML can only provide a minimum-limiting age for the desert pavement. Thus, the oldest VML age provides a minimum age for the underlying desert pavement.

3.3.4. Strontium isotopes to assess the origin of the Av horizon

Dust deposition occurs regularly in association with Arizona summer monsoon season (Brazel, 1989; Marcus and Brazel, 1992). Furthermore, the strong seasonality of natural flows in the Salt and Verde Rivers produced extensive braided floodplains for local deflation of desiccated suspended sediment (Honker, 2002). Thus, the terraces of the Salt and Verde rivers would have been subjected to both locally and regionally derived dust. Because strontium isotopes have the potential to discriminate source materials (Capo et al., 1998; Capo and Chadwick, 1999), ^{87}Sr/^{86}Sr ratios assessed the hypothesis that the fine material underneath terrace desert pavements derived from this dust and not the underlying alluvial deposit

A Nuclide 1290 mass spectrometer measured ^{87}Sr/^{86}Sr ratios in the following types of samples collected in a depth profile from the surface down:

- dust collected from the surface depressions of pavement cobbles;
- the upper half of the Av horizon;
- the lower half of the Av horizon;
- for the Stewart Mountain and Lousley Hills terraces lacking an Av horizon, A horizon medium sand collected directly underneath surface clasts; some cobbles from the Mesa Verde terrace also lacked an Av, and sand was collected under these cobbles
- Bw horizon material collected ~5 cm underneath the A or Av horizon
- Bk horizon material collected ~50 cm underneath the surface
- amalgamation of three sets of 10 cobbles, then subject to HCl to remove carbonate rinds, and then pulverized; collected ~50 cm underneath the surface

Each of these samples were separated into the acetic acid-soluble fraction that represents carbonate and labile Ca and the silicate fraction. Samples were normalized to the ^{87}Sr/^{86}Sr ratio of 0.1194 and compared to the Eimer and Amend standard (0.7080).

Table 7
^{10}Be exposure ages of cobbles and a pair of ^{10}Be-^{26}Al analysis of one burial sample (Sawik021) on terraces of the Salt and Verde Rivers.

Sample	Lithology[a]	Latitude (°N; WGS84)	Longitude (°W; WGS84)	Elevation (m)	Thickness (cm)[b]	Shielding factor[d]	^{10}Be concentration (10^5 atoms g^{-1} SiO_2)[e,f]	^{10}Be concentration (10^5 atoms g^{-1} SiO_2)[g]	Exposure age (ka)[h,i,j]	Exposure age (ka)[k]	Terrace age (ka)[l]	^{26}Al concentration (10^5 atoms g^{-1} SiO_2)[m]	Source
Mesa001	Gneiss	33.53996	111.62935	461	4	0.99	7.70 ± 0.28	5.02 ± 0.18	91.5 ± 8.8	94.9 ± 9.1	85.8 ± 2.0		Larson et al. (2017)
Mesa002	Gneiss	33.53988	111.62924	462	5.5	0.99	6.83 ± 0.87	4.15 ± 0.52	76.3 ± 11.9	79.1 ± 12.4			
Mesa003	Granite	33.53999	111.62936	459	5	0.99	6.19 ± 0.37	3.51 ± 0.21	64.3 ± 6.8	66.6 ± 7.1			
Mesa004	Quartzite	33.53991	111.62922	458	4.5	0.99	7.09 ± 0.45	4.41 ± 0.28	80.8 ± 8.9	83.7 ± 9.2			
Mesa005	Granite	33.53992	111.62933	460	4.5	0.99	7.88 ± 0.46	5.20 ± 0.30	95.4 ± 10.2	98.9 ± 10.6			
Mesa006	Granite	33.53999	111.62952	458	4	0.99	9.68 ± 0.50	7.00 ± 0.36	129.2 ± 13.5	133.9 ± 14.0			
Mesa007	Mixture	33.53951	111.62856	450	Deep[c]		2.67 ± 0.09	Inheritance	Inheritance	Inheritance			
MesaV045	Quartzite	33.66484	111.69253	496	3	0.99	5.09 ± 0.31	3.70 ± 0.12	64.7 ± 2.1	67.0 ± 6.3	46.0 ± 23.2		This study
MesaV046	Gneiss	33.66486	111.69258	494	5	0.99	3.11 ± 0.11	1.72 ± 0.06	30.4 ± 1.15	31.5 ± 3.0			
MesaV047	Gneiss	33.66489	111.6926	495	4	0.99	3.97 ± 0.14	2.58 ± 0.09	45.3 ± 1.6	46.9 ± 4.4			
MesaV048	Gneiss	33.66486	111.69267	497	5	0.99	2.72 ± 0.16	1.34 ± 0.08	23.6 ± 1.4	24.4 ± 2.6			
MesaV049	Granite	33.66499	111.69298	496	6	0.99	5.97 ± 0.24	4.59 ± 0.18	82.5 ± 3.4	85.5 ± 8.3			
MesaV050	Granite	33.66501	111.69302	496	4.5	0.99	3.08 ± 0.14	1.69 ± 0.07	29.7 ± 1.3	30.7 ± 3.0			
SM037	Gneiss	33.57004	111.63284	525	3	0.99	7.55 ± 0.31	6.17 ± 0.26	106.6 ± 4.6	110.4 ± 10.9	82.7 ± 2.4		This study
SM038	Gneiss	33.57041	111.63264	524	4	0.99	5.89 ± 0.19	4.50 ± 0.14	77.9 ± 2.6	80.8 ± 7.6			
SM040	Gneiss	33.57214	111.63015	520	4.5	0.99	7.93 ± 0.51	6.55 ± 0.42	115.1 ± 7.7	119.4 ± 13.3			
SM041	Granite	33.57112	111.62885	522	4.5	0.99	4.69 ± 0.14	3.31 ± 0.10	57.2 ± 1.8	59.2 ± 5.5			
SM042	Granite	33.56667	111.62941	522	1.5	0.99	4.70 ± 0.16	3.31 ± 0.11	57.4 ± 2.1	59.4 ± 5.6			
SM043	Quartzite	33.57004	111.63284	525	3	0.99	6.20 ± 0.25	4.81 ± 0.19	81.8 ± 3.4	84.8 ± 8.3			
LH028	Granite	33.7056	111.70166	618	5	0.99	2.61 ± 0.11	1.23 ± 0.05	19.6 ± 0.8	20.3 ± 1.9	16.6 ± 1.1		This study
LH029	Granite	33.70545	111.70614	620	4	0.99	2.01 ± 0.09	0.62 ± 0.03	9.8 ± 0.4	10.2 ± 1.0			
LH030	Gneiss	33.70548	111.70161	618	5	0.99	1.79 ± 0.08	0.41 ± 0.02	6.5 ± 0.3	6.7 ± 0.6			
LH031	Gneiss	33.70573	111.70619	618	5	0.99	2.63 ± 0.13	1.25 ± 0.06	20.0 ± 1.0	20.7 ± 2.0			
LH032	Granite	33.70577	111.70171	618	5	0.99	2.30 ± 0.09	0.92 ± 0.03	14.7 ± 0.6	15.3 ± 1.4			
LH033	Gneiss	33.70541	111.70163	619	4	0.99	1.78 ± 0.09	0.37 ± 0.02	5.9 ± 0.3	6.1 ± 0.6			
LH034	Quartzite	33.70548	111.70163	620	7	0.99	3.83 ± 0.21	2.44 ± 0.13	39.8 ± 2.2	41.2 ± 4.3			
BP008	Granite	33.55286	111.57689	434	3.5	0.99	3.33 ± 0.30	1.93 ± 0.17	35.3 ± 4.4	36.6 ± 4.6	30.7 ± 1.0		Larson et al. (2017)
BP010	Granite	33.55286	111.57689	434	4.6	0.99	3.26 ± 0.19	1.85 ± 0.10	34.2 ± 3.6	35.5 ± 3.7			
BP011	Gneiss	33.55286	111.57689	434	4	0.99	5.05 ± 0.27	3.65 ± 0.19	67.6 ± 7.0	70.0 ± 7.3			
BP012	Gneiss	33.55286	111.57689	434	5.8	0.99	3.25 ± 0.24	1.84 ± 0.13	34.3 ± 3.9	35.5 ± 4.1			
BP013	Granite	33.55286	111.57689	434	5.4	0.99	2.47 ± 0.19	1.07 ± 0.08	19.8 ± 2.3	20.5 ± 2.4			
BP014	Mixture	33.55286	111.57689	429	Deep[c]		1.40 ± 0.08	Inheritance	Inheritance	Inheritance			
Sawik015	Quartzite	33.48903	111.71483	438	4.5	0.99	18.07 ± 0.44	16.24 ± 0.40	320.5 ± 8.6	332.9 ± 32.6	332.0 ± 4.1		This study
Sawik016	Granite	33.48903	111.71483	439	6.5	0.99	19.02 ± 0.60	17.19 ± 055	346.9 ± 12.1	360.4 ± 36.4			
Sawik017	Quartzite	33.48903	111.71483	439	4	0.99	18.18 ± 0.57	16.35 ± 0.51	321.4 ± 10.9	333.8 ± 33.4			
Sawik018	Granite	33.48903	111.71483	437	4.5	0.99	20.12 ± 0.52	18.28 ± 0.47	364.7 ± 10.3	378.9 ± 37.6			
Sawik019	Geniss	33.48903	111.71483	439	5.5	0.99	19.01 ± 0.48	17.18 ± 0.44	343.6 ± 9.6	357.0 ± 35.2			
Sawik020	Gneiss	33.48903	111.71483	438	4.5	0.99	17.2 ± 0.52	15.44 ± 0.46	303.3 ± 9.9	315.0 ± 31.2			
Sawik021	Mixture	33.48903	111.71483	438	Deep[c]		1.35 ± 0.07	Inheritance	Inheritance	Inheritance		6.70 ± 0.19	

Note:
[a] The tops of all samples were exposed at the terrace surface.
[b] Whole cobble was used considering possible multiple turnaround since initial abandonment.
[c] Amalgamated (n > 30) cobbles were sampled from deep (>5 m) depth.
[d] Geometric shielding correction for topography was measured on an interval of 10°.
[e] Uncertainties are reported at the 1σ confidence level.
[f] Propagated uncertainties include error in the blank, carrier mass (1%), and counting statistics.
[g] Inheritance yielded from a mixture (n > 30) of cobble at depth (*e.g.* Mesa007, BP014, and Sawik021) is corrected for calculating pure production since abandonment.
[h] All ages are corrected for inheritance and expressed with 1 sigma external uncertainty.
[i] Beryllium-10 model ages were calculated using global production rate of 4.49 ± 0.39 at SLHL with the Cosmic-Ray Produced Nuclide Systematics (CRONUS) Earth online calculator version 2.2 (http://hess.ess.washington.edu/).
[j] Propagated error in the model ages include a 6% uncertainty in the production rate of ^{10}Be and a 4% uncertainty in the ^{10}Be decay constant.
[k] Ages were calculated using North America regional production rate of 4.33 ± 0.21 (Balco et al., 2009).
[l] Weighted mean of ages calculated using global production rate and error within the 1σ confidence level.
[m] Measured for the same sample of which ^{10}Be (Sawik021) abundance was measured for yielding maximum burial age assuming one simple burial event of all cobbles analyzed.

3.4. Results

3.4.1. Cosmogenic nuclides

^{10}Be exposure ages of the terraces and their scatters are widely different depending on their locations and characteristics (Table 7). The Mesa and Blue Point terrace ^{10}Be ages for pavement cobbles were published previously (Larson et al., 2017) in the context of a study of pediments graded to these terrace remnants. The other data in Table 7 are new. Relatively, the strath terraces in the Salt River are better constrained in that they have 8–80 times lower Mean Square Weighted Deviation (MSWD or reduced chi-square in Fig. 4) than the ones in the Verde River. Pavement cobbles have weighted means of 30.7 ± 1.0 ka, 85.8 ± 2.0 ka, 332.0 ± 4.1 ka for Blue Point, Mesa, and Sawik terraces, respectively, whereas pavement cobbles on the topographically higher (and clearly older) Stewart Mountain terrace yields much younger age (82.7 ± 2.4 ka) than expected, based on the relative stratigraphy (Fig. 4).

Pavement cobbles on the terraces in the Verde River yield much younger ages with greater scatter than the coeval levels of terraces in the Salt River. The age of cobbles on the Mesa Verde terrace are widely scattered with weighted mean age of 46.0 ± 23.2 ka. We highlight that the highest and hence oldest terrace on the Lousely Hill (Fig. 4) yields the youngest ages for pavement cobbles (16.6 ± 1.1 ka).

Probability plots (sometimes called camel plots) have been a standard way of visualizing exposure ages in using cosmogenic nuclides for dating (Small and Fabel, 2016). The camel plots for the terrace pavements shown in Fig. 8 display two types of information. The dashed lines show the individual probabilities for each pavement cobbles. By convention, uncertainties used to generate individual probability curves are 1σ analytical uncertainties. The thicker solid line shows the

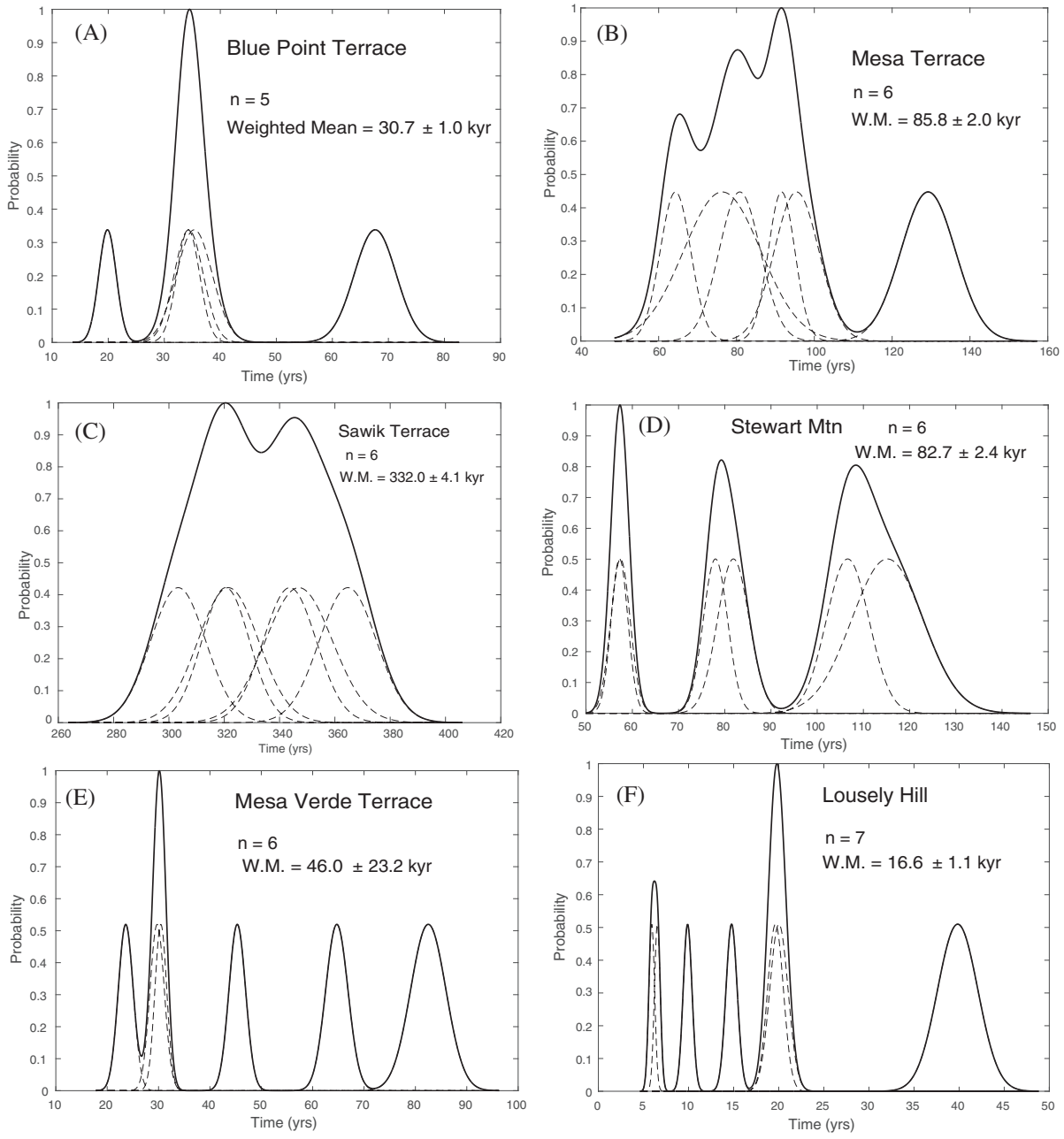

Fig. 8. Probability plots of ages of terraces along the Salt and the Verde River. (A) Blue Point terrace, (B) Mesa terrace, (C) Sawik terrace, (D) Stewart Mountain terrace, (E) Mesa Verde terrace, and (F) Lousely Hill terrace. All ages are weighted mean and error at 1σ confidence interval.

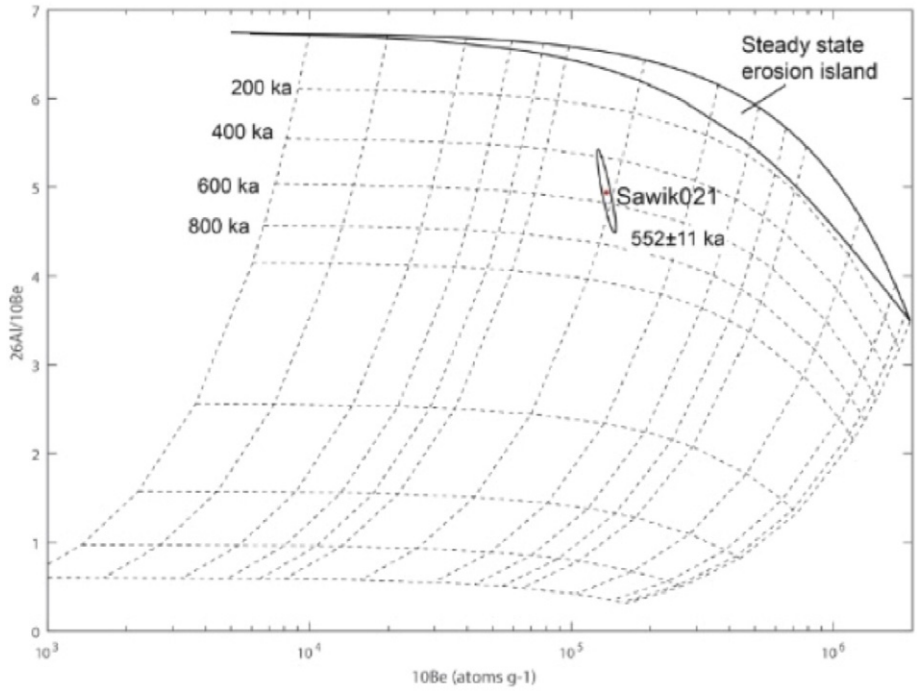

Fig. 9. Sample burial age of the Sawik terrace. The age is modeled assuming one depositional event and zero surface erosion.

cumulative probability. The cumulative probability line allows the reader to quickly visualize the distribution of ages. For example, the Sawik terrace (Fig. 8C), single hump in the probability plot implies that the sampled gravels would have been relatively stable on the surface since the timing of terrace abandonment (332.0 ± 4.1 ka). In contrast, the multiple humps for the topographically higher Stewart Mountain terrace suggests that the sampled pavement cobbles periodically eroded out of the underlying alluvium between 50 and 120 ka.

After obtaining initial ^{10}Be abundance produced during prior exposure from a mixture of gravels (n > 30) at depth (>5 m) for desert pavement cobbles on the Sawik terrace, its ^{26}Al abundance was also measured to constrain the burial age of the terrace deposit. The age calculation assumes one depositional event with zero surface erosion (Fig. 9). The sample of buried gravels was collected from a road cut directly on top of the granitic strath (Fig. 6I) and first provides a maximum age for the overlying pavement. One scenario is that the analyzed sediments experienced some history of prior burial before being finally deposited on the Sawik strath — setting a lower ratio of ^{26}Al/^{10}Be than the continuous exposure case with ratio of ~6.7. A second scenario is that the burial age reflects the timing of when the ancestral Salt River last abraded this granitic strath and that the very surface of the Sawik terrace was abandoned well after deposition of these buried cobbles. Any combination of different factors (burial age could be younger than the ~552 ka maximum; some surface erosion occurred prior to pavement stabilization; lengthy time between deposition of buried cobbles and abandonment of terrace) could also explain the *ca.* 220 ka time difference between the burial age (Fig. 9) and the surface exposure age of pavement cobbles (Fig. 8C).

In an effort to better constrain the exposure history of cobbles on top of the Sawik pavement, we also analyzed *in situ* ^{14}C in the quartzite cobbles in the same three cobles also measured for ^{10}Be buildup (Table 8). Bioturbation burying the cobbles for a period of time would reduce the *in situ* ^{14}C below levels of saturation. However, if the cobbles remained at the surface for the last ~20 ka, *in situ* ^{14}C would be at saturation and all samples would plot in the steady-state erosion island of Lal (1991).

Two of three samples were measured successfully, and both cobbles (Sawik017 and Sawik020) are plotted in the steady-state erosion island within uncertainty. Thus, it is likely that both cobbles experienced limited burial for a time >1 ka during the last ~20 ka (Fig. 10). The most likely cause would be accumulation of aeolian material from the nearby Salt River floodplain. The burial could have been one event a bit more than a millennia or repeated burial events lasting centuries or decades. Although it is difficult to be certain from just two measurements, the ability to track the burial history of pavement cobbles using *in situ* ^{14}C

Table 8
Results of *in-situ* produced cosmogenic ^{14}C. All the errors are 1σ. All the processes for calculating ^{14}C atoms *in-situ* produced in quartz are based on the equations in prior research (Donahue et al., 1990).

Sample	Lab ID	Quartz (g)	$\delta^{13}C_{meas}$ [a]	F[b]	CO_2 yield (μL)[c]	Dead $CO_{2(mL)}$[d]	^{14}C (10^5 atoms g^{-1})	^{14}C/^{10}Be
Sawik017	KU151205	5.26	−30.2400	0.0432	36.9	1.5162	1.97 ± 0.48[e]	0.10 ± 0.01
Sawik018	KU151206	5.15	−39.1828	0.0335	43.5	1.4753	Failed	Failed
Sawik020	KU151204	5.20	−35.8799	0.0328	8.2	1.5582	1.69 ± 0.52[f]	0.09 ± 0.01

[a] Used for calibration with NIST oxalic acid (^{14}C/^{12}C: 134 pMC) $\delta^{13}C = -17.8‰$).
[b] Calculation of fraction modern corrected for background (dead CO_2) with average (n = 6) value of 0.0012. Uncertainty causing from pressure gauge is 2.3 μg.
[c] Total CO_2 extracted from quartz with step-wise collection and purification.
[d] Low ratio ($<3 \times 10^{-15}$) of background carrier spiked.
[e] Corrected for process blank with a mean ^{14}C concentration of 9.46 (± 0.32) × 10^5.
[f] Corrected for process blank with a mean ^{14}C concentration of 6.33 (± 2.01) × 10^5.

opens up an entirely new strategy to understand the trajectories of rocks in all different types of surficial cobbles — whether the cobbles occur in warm desert pavements or archaeological quarries. In this case, burial about 5% of the time in the last 20,000 years indicates that flotation by dust must not be the only process in operation.

3.4.2. OSL

The OSL ages of the two Blue Point terrace samples (Table 9) are consistent with the ^{10}Be cosmogenic nuclide ages for the pavement cobbles of 30.7 ± 1.0 ka (Table 7), since the deposition of the sandy lenses underneath the surficial cobbles should predate terrace abandonment and the start of pavement formation. Similarly, these new results are consistent with the calibrated ^{14}C age of 33,100 ± 380 calendar years for the innermost carbonate rind around gravel in the Bk horizon (Larson et al., 2010), since this pedogenic Stage 1 carbonate only started to form after the strath terrace surface was abandoned upon Salt River incision.

3.4.3. Soil profiles and varnish microlaminations

Soil profile analyses (Table 10) presents the sequence of soil development on the Mesa River terraces. The depth of the profile was limited for the Mesa and Sawik terraces by encountering a Stage IV petrocalcic horizon, but the Stage I development in the Blue Point reached a depth of 70 cm.

Table 10 presents only the oldest VML ages obtained from three terraces of the Salt River. Because cobble spalling resets the varnish clock, all younger ages only reflect the spalling event. The oldest VML calendar age for the Blue Point terrace of 30 ka (Table 5) is slightly younger than the calibrated ^{14}C age carbonate rind age, the ^{10}Be surface exposure age on pavement cobble, and is substantially younger than the OSL ages for sandy deposits beneath the pavement. Thus, the sampled cobble stabilized at the surface by at least 30 ka.

The oldest VML calendar age for the Mesa terrace of calendar 74–85 ka (Table 5) is consistent with ^{10}Be surface exposure age on pavement cobbles. Again, this minimum exposure age means that the sampled cobble stabilized at the surface at least in the time range of 74–85 ka.

The oldest VML calendar age for a cobble sampled from the Sawik terrace is 74–85 ka (Table 10). This is much younger than the ^{10}Be surface exposure age on pavement cobbles, meaning that the surface of the cobbles have been experiencing spalling of at least a millimeter of rock to reset the varnish clock.

3.4.4. Strontium isotopes to assess the origin of the Av horizon

The ^{87}Sr/^{86}Sr analyses of the carbonate and silicate fractions of dust collected from depressions on pavement rocks rests at one end with ^{87}Sr/^{86}Sr ratios ~0.71 (Table 11 and Fig. 11). In contrast, the pulverized rock material making up the terrace alluvium maintains very different ^{87}Sr/^{86}Sr ratios ranging from ~0.73 to ~0.75. In interpreting the results in Fig. 11, we consider the dust and pulverized alluvium to be "end members". In Fig. 11 the pulverized clasts sampled from a 50 cm depth show ^{87}Sr/^{86}Sr ratios ranging from 0.73 to 0.75. In contrast, dust resting on the surface has ^{87}Sr/^{86}Sr ratios centered around 0.71.

With the perspective of dust at one end of the ^{87}Sr/^{86}Sr spectrum and the host rock material of the terrace alluvium at the other end, some basic qualitative inferences can be made. (a) The carbonate fraction extracted in the HCl leachate in all materials appears to derive mostly from the dust, although a small amount of the carbonate in the Bw and Bk horizons could derive from calcium chemically dissolved from terrace alluvium. (b) The silicate fraction in the Av horizons derives from dust. (c) The silicate fraction of the sandy A-horizon underneath Lousley Hills, Stewart Mountain, and a few Mesa Verde cobbles appear to derive from the alluvium; and (d) the silicate fraction of the Bw and Bk horizons yields a mixed signal and appears to derive from both infiltrating dust and alluvium.

The ^{87}Sr/^{86}Sr analyses presented in Table 11 and Fig. 11 indicate that there are two sources for the fines underneath the studied Sonoran Desert pavements. The ^{87}Sr/^{86}Sr analyses of the Av horizons and the carbonate fraction shows a clear aeolian signature. In contrast, alluvium-sourced materials contribute to Bw, Bk, and sandy A-horizons where Av-horizons are lacking.

4. Factors involved in desert pavement longevity or mortality

4.1. Minimal surface topography

The desert pavement atop the Sawik terrace of the Salt River (Fig. 6G–I) is the oldest known pavement in the Sonoran Desert at ~332 ± 4 ka, and the desert pavement atop the Mesa terrace of the Salt River

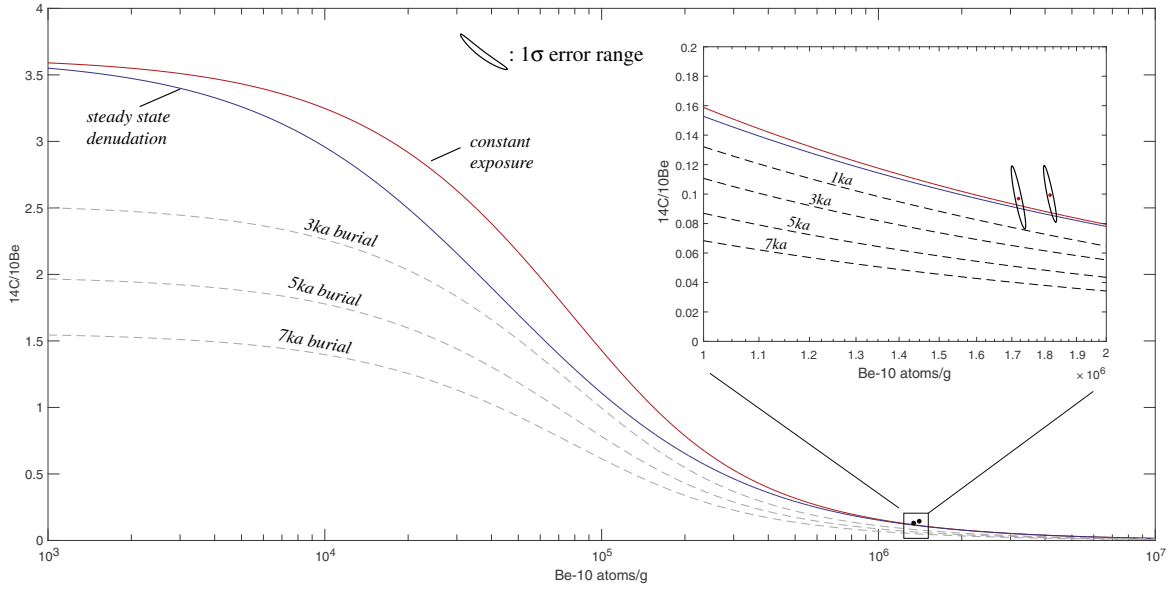

Fig. 10. A pair of ^{10}Be and ^{14}C analysis of two cobbles on the Sawik pavement. Both samples are plotted within steady-state erosion island (Lal, 1991) assuming uncertainty or were not buried for longer than 1 ka for the last ~20 ka.

Table 9
Equivalent doses (De), dose rate and OSL ages of Blue Point terrace samples.

Sample	Water content[a] (%)	Dose Rate (Gy/ka)	Equivalent dose (Gy)	Aliquots used[b] (n/N)	OSL age (ka, 1σ SE)
BPO-001	7.3 (30.6)	3.62 ± 0.09 (2.90 ± 0.07)	159 ± 3	16/16	44 ± 1 (55 ± 2)
BPO-002	6.0 (28.5)	4.07 ± 0.10 (3.27 ± 0.08)	131 ± 2	15/16	32 ± 1 (40 ± 1)

Note:
[a] Numbers in parenthesis were those calculated based on saturated water contents.
[b] n/N refers to the ratio of (the number of aliquots used for data analysis)/(total number of aliquots loaded in the OSL measurement system).

(Fig. 6D-F) is the second oldest known pavement at ~86 ± 1 ka. Both Sawik (Fig. 6G-I) and Mesa (Fig. 6D-F) terrace fragments have in common low slopes, of less than a degree.

Low relief has long been known to be important in pavement stability (Cooke, 1970; Peterson, 1981; Dixon, 1994). Stable Negev Desert pavements have little local relief (Dan et al., 1982; Matmon et al., 2009; Amit et al., 2011), as does the >3 Ma old pavement in the Atacama Desert (Placzek et al., 2014) as well as ancient pavements elsewhere (Fukioka and Chappell, 2011). Pavement genesis smoothing processes play a role in promoting low relief and proceed on alluvial fans in the Mojave Desert for ~56 ka (Oskin et al., 2007), in Death Valley for ~70 ka (Frankel and Dolan, 2007), and for >280 ka in the Coachella Valley (Matmon et al., 2006).

In contrast, sloping surfaces in the Cima Volcanic field (Wood et al., 2005) and in the Libyan Desert (Adelsberger and Smith, 2009; Adelsberger et al., 2013) are associated with pavement instability. The rounding of alluvial fans has long been known as a cause of pavement instability (Field and Pearthree, 1997). This is certainly the case for the two highest terraces of the Salt (Fig. 5F) and Verde Rivers (Fig. 5D). The Stewart Mountain and Lousley Hills (Fig. 4) high terraces host gently rounded hillcrests well above the surrounding topography. The ongoing exposure of previously buried clasts is a common and reasonable explanation for clast ^{10}Be ages (Fig. 8D, F) far younger than their geomorphological position would indicate.

4.2. Hyperaridity

The oldest known pavements occur in regions experiencing long-term hyperaridity (Matmon et al., 2009; Placzek et al., 2014; Wang et al., 2015). Gypsum (and carbonate) precipitation contributes to pavement stability in hyperarid regions of the Negev Desert (Amit et al., 2010; Boroda et al., 2013), Precordillera of Argentina (Hedrick et al., 2013), and Atacama Desert in Chile (Dunai et al., 2005; Clark, 2006; Evenstar et al., 2009; Matmon et al., 2009; Wang et al., 2015).

Our case study of Salt River and Verde River terraces exist pavements, however, exist in a region that experienced conditions other than aridity in the past. The terraces sites in Sonoran Desert experienced prolonged semi-arid conditions during the last glaciation (McAuliffe and Van Devender, 1998). Similarly, the ancient pavements on Nevada lava flows (Zreda et al., 1993; Heizler et al., 1999; Valentine and Harrington, 2006; Valentine et al., 2006) experienced much wetter conditions during the last glacial cycle (Wells, 1983; Benson and al, 1990). In another example, pavements that are ~71–72 ka in Wyoming (Anderson et al., 1996) experienced several glaciations in the area

Table 10
Soil profiles of the Blue Point, Mesa, and Sawik terraces of the Salt River; soils data collected with Troy Péwé.

Horizon	Blue Point	Mesa	Sawik
Soil	Typic Haplargid	Petrocalcic Calciorthid	Petrocalcic Calciorthid
Desert pavement	90% pebbles and cobbles with the oldest rock varnish VML[a] sequence of LU-1/LU-2/LU-3/LU-4 (WP3) minimum age 30 ka	85% pebble and cobbles with the oldest rock varnish VML sequence of LU-1/…/LU-4/LU-5 (WP6+) minimum age 74–85 ka	95% cobbles with the oldest rock varnish VML sequence of LU-1/…/LU-4/LU-5 (WP6+) minimum age 74–85 ka
Av	1–3 cm; light yellowish brown (10 years 6/4); dry; many vesicular pores, weak platy structure; soft, slightly sticky (wet); few fine roots; slightly effervescent; moderately alkaline (pH 8.0); clear smooth boundary	2–5 cm; light yellowish brown (10 years 6/4); dry; many vesicular pores, weak platy structure; slightly hard, friable; nonsticky and nonplastic (wet); common fine roots; slightly effervescent; moderately alkaline (pH 8.2); abrupt smooth boundary	2–7 cm; light yellowish brown (10 years 6/4) dry; many vesicular pores, weak platy structure; slightly sticky; nonsticky and nonplastic (wet); few fine roots; slightly effervescent; moderately alkaline (pH 8.0); abrupt smooth boundary
Bw	1–4 cm; light brown 7.5 years 6/4; dry; fine sandy loam; weak fine granular structure; soft, friable, slightly sticky (wet); rock fragments completely coated with carbonate; 30% pebbles; violent effervescent; moderately alkaline (pH 8.1); clear wavy boundary	8 to 20 cm; reddish brown (5 years 5/4); dry; massive; friable, slightly hard, slightly sticky and slightly plastic (wet); common fine roots; common fine interstitial pores; 50% pebbles; strongly effervescent; moderately alkaline (pH 8.3); clear wavy boundary	2 to 12 cm; reddish brown (5 years 5/4); dry; massive; friable, slightly hard, slightly sticky and slightly plastic (wet); few fine roots; few very fine interstitial pores; 70% pebbles; strongly effervescent; moderately alkaline (pH 8.1); clear wavy boundary
Bk	5 cm to 70 cm; pale brown (10 years 6/3)dry ; extremely gravelly loam; massive; soft, very friable; nonsticky, nonplastic (wet); few fine roots; 80% pebbles; common thin carbonate coatings covering pebbles; strongly effervescent; moderately alkaline (pH 8.1); abrupt wave boundary	10 cm to 90 cm; light brown (7.5 years 6/4) dry; loose to very friable; slightly sticky and slightly plastic (wet); few fine roots; common fine interstitial pores; 60% pebbles; common carbonate coatings covering and bridging pebbles; violently effervescent; moderately alkaline (pH 8.1); abrupt smooth boundary	5 cm to 50 cm; light brown (7.5 years 6/4) dry; loose to very friable; non sticky and slightly plastic (wet); few fine roots; common fine interstitial pores; 60% pebbles; common carbonate coatings covering and bridging pebbles; violently effervescent; moderately alkaline (pH 8.0); abrupt smooth boundary
Bkm	Not present	90 cm - pinkish white (7.5 years 8/2) dry; massive; extremely hard; extreme violet effervescence (Stage IV carbonates)	50 cm - pinkish white (7.5 years 8/2) dry; massive; extremely hard; extreme violet effervescence (Stage IV carbonates)
Cr	Observed in stream cuts at depth ~4 m partially weathered granite; common thin carbonate veins in fractures; abrupt wavy boundary	Observed in road cuts at depth ~5 m partially weathered granite; common thin carbonate veins in fractures; abrupt wavy boundary	Observed in road cut at depth ~4 m partially weathered granite; common thin carbonate veins in fractures; abrupt wavy boundary

[a] VML sequence nomenclature follows Liu and Broecker (2008a, 2008b).

Table 11
$^{87}Sr/^{86}Sr$ analyses from the Salt River and Verde River terrace. Each datum represents a single analysis from samples collected in a soil pit. The samples from each depth were first subject to HCl to first analyze only the carbonate fraction; the remaining silicate remainder was then analyzed separately. Each depth profile starts with dust collected from the surfaces of pavement rocks, continues into the upper half of the Av horizon, lower half of the Av horizon, B horizon, and then C horizon. Since the Stewart Mountain, Verde Mesa, and Verde Lousley Hills terraces either lacked an Av horizon or had only a very thin Av horizon, medium sand was sampled instead directly underneath surface boulders. Each pulverized rock sample collected from the C horizon represent an amalgamation of 10 different clasts.

$^{87}Sr/^{86}Sr$ sampled landform	Salt Blue Point	Salt Mesa	Salt Sawik	Salt Stewart Mtn	Verde Mesa	Verde Lousley Hills
Coordinates	N 33.55273 W 111.57816	N 33.53986 W 111.62907	N 33.48950 W 111.71280	N 33.57167 W 111.63179	N 33.66457 W 111.69182	N 33.70105 W 111.71001
Surface dust HCl leachate	0.708946	0.707483	0.706944	0.707119	0.708216	0.707722
Surface dust silicate	0.711155	0.711504	0.711552	0.712489	0.711715	0.711867
Av upper layer dust HCl leachate	0.709011	0.708032	0.708843	0.709274	0.70878	No Av
Av upper layer silicate	0.711094	0.712261	0.711785	0.711985	0.711783	No Av
Av lower layer dust HCl leachate	0.710018	0.709459	0.709767	Only thin Av	Only thin Av	No Av
Av lower layer silicate	0.711113	0.711870	0.712369	Only thin Av	Only thin Av	No Av
A medium sand 1 cm under boulders HCl leachate	No sandy layer	No sandy layer	No sandy layer	0.71249	0.713382	0.711894
A medium sand 1 cm under boulders silicate	No sandy layer	No sandy layer	No sandy layer	0.731442	0.750222	0.749513
Bw 5 cm under A HCl leachate	0.709157	0.712055	0.71147	0.71406	0.716388	0.711029
Bw 5 cm under A silicate	0.71152	0.710922	0.711341	0.722913	0.739578	0.748112
Bk 50 cm under A HCl leachate	0.709229	0.709442	0.712273	0.717302	0.716029	0.718124
Bk 50 cm under A silicate	0.711665	0.712022	0.713961	0.730028	0.731155	0.742057
Bk 50 cm pulverized rock	0.730430	0.728441	0.731148	0.740109	0.751139	0.743520
Bk 50 cm pulverized rock	0.732662	0.730105	0.735229	0.741225	0.747872	0.735220
Bk 50 cm pulverized rock	0.727511	0.727004	0.734633	0.735790	0.739884	0.745492

(Phillips et al., 1997). Thus, while hyperaridity appears needed for the survival of pre-Quaternary pavements, it is clearly (Table 11) not a requirement for Pleistocene antiquity.

4.3. Ongoing input of allochthonous dust

Strontium isotope data collected at the Sawik and Mesa terrace sites reveals the presence of dust on pavement cobbles, under pavement clasts in the Av horizon, and infiltrating down into the Bw and Bk soil horizons (Table 11 and Fig. 11). Mineralogical analyses on Av horizons in southern Jordan similarly revealed an aeolian origin (Ugolini et al., 2008). These findings are similar to the Mojave and western Sonoran Deserts, where the source of the aeolian material in vesicular horizons derives from distal washes of alluvial fans as well as playas (Sweeney et al., 2013). Consistent with our ^{10}Be age of ~335 ka for the Sawik terrace, flotation of desert pavements by dust accumulation (Mabbutt, 1977; Mabbutt, 1979; Gerson and Amit, 1987; McFadden et al., 1987) plays a key role in pavement stability according to other cosmogenic nuclide and OSL studies (Shepard et al., 1995; Wells et al., 1995; Matmon et al., 2009; Guralnik et al., 2010; Amit et al., 2011; Fisher et al., 2014; Fuchs et al., 2015; Wang et al., 2015).

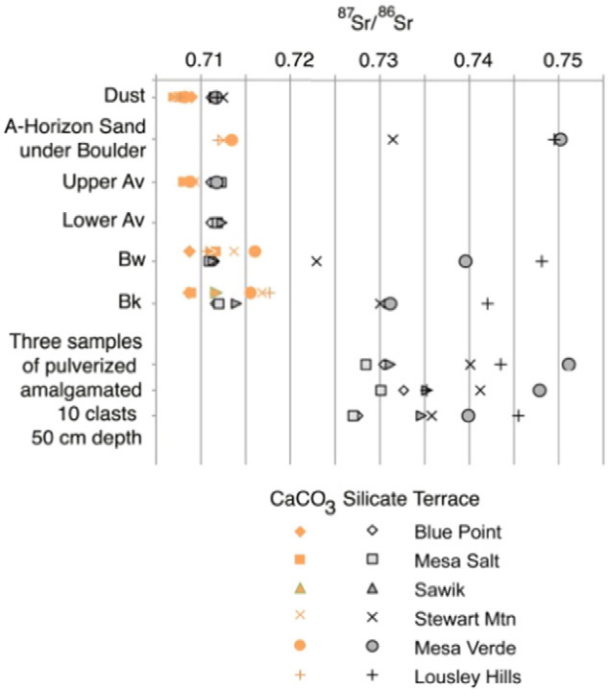

Fig. 11. $^{87}Sr/^{86}Sr$ analyses organized according to depth in a soil profile and whether the analysis was conducted on the HCl leachate (carbonate fraction) or the remaining silicate fraction. The A-horizon sand underneath sampled boulders and cobbles is the equivalent depth to the Av horizons, because this sandy material was collected where there was no Av horizon. Bw and Bk samples were collected from 5 and 50 cm beneath the Av horizon and the surface, respectively. Thirty cobbles were also collected at the 50 cm depth in the Bk horizon, grouped into 3 sets of ten, and pulverized to create amalgamation samples.

Concomitantly, the Sonoran Desert terrace case study also reveals that pavements that are not floated by dust and are instead underlain by sand are not stable geomorphologically. Pavements underlain by sand on the Stewart Mountain, Lousley Hills, and the Mesa terrace along the Verde River (Table 11 and Fig. 11) experience ongoing erosion and cosmogenic ages far younger than their geomorphic position (Fig. 8E-F). In these settings, the sand has a strontium-isotope signal consistent with derivation from the underlying terrace alluvium and not infiltrated dust (Table 11 and Fig. 11).

4.4. Lack of headward-retreating swales

The Sawik and Mesa terrace remnants do not display evidence of headward-retreating gullies or even swales. Even subtle swale development on terraces can mix highly and more recently exposed cobbles in the Tian Shan, China (Huang et al., 2014), as well as Oman and UAE (Al-Farraj and Harvey, 2000). In Death Valley, USA, "[g]ully incision into units older than 70 ka occurs, decreasing pavement stability as the fan material erodes" (Frankel et al., 2007a). However, the pavement on the Mesa terrace along the Verde River (Fig. 7A) shows signs of instability due to development of swales on its surface, likely exposing formerly buried clasts and generating the age distribution seen in Fig. 8E.

4.5. Lack of or minimal biotic disturbance

Matmon et al. (2009) emphasized a lack of biotic disturbance as a possible explanation for long-lived pavements. Bioturbation has long been known to impact the stability of desert pavements (Parker, 1991; Huckleberry, 1993, 1994; Quade, 2001). Research in the Mojave

Desert indicates that there could be two distinct pathways for surface evolution in a desert: "abiotic landform evolution" and "biological landform evolution", where each pathway results in different landform systems on alluvial fans (Pietrasiak et al., 2014). This "fork in the road" hypothesis works well with vegetation and soil-geomorphic surface mosaics in the Mojave and Sonoran deserts (Musick, 1975; Wood et al., 2005).

In the Sonoran Desert case study, we purposefully avoided locations of active bioturbation and old plant scars (Dickerson and Cocks, 2015). In Arizona, increases in elevation and a greater abundance of perennial plants in cooler and wetter conditions are generally associated with a reduction in a landform's maintenance of a desert pavement above an elevation of 550 m (Huckleberry, 1993, 1994).

A similar elevation-based trend has been noted elsewhere in the southwestern USA (Quade, 2001). The exact mechanism of pavement disturbance varies from site to site. Animal foraging activities disrupts desert pavement on the Salt and Verde terraces on unknown timescales, but these disturbances are rare (inferred to be on millennial time scale) in Death Valley (Haff, 2001). At Stonewall Flat Nevada, sand and silt accumulating around larger shrubs host animal burrows (Dickerson et al., 2013). We also noticed soil biological crusts associated with pavement disturbance, and older alluvial surfaces where pavement has started to erode develops scattering of moss-lichen biological soil crust pinnacles (Williams et al., 2013). Thus, while some argue for a climate limit to pavement survival (Quade, 2001), we view site selection to be critically important in understanding pavement age limits as evidenced by research demonstrating that ancient pavements can and do occur outside Quade's (2001) climatic limits (Anderson et al., 1996; Valentine and Harrington, 2006).

4.6. Bedrock beneath the pavement

Locations where bedrock exists directly underneath pavements can lead to long-term stability. Mabbutt (1977) recognized that the hamadas and gibber plains formed on top of bedrock tend to be stable. Buildup of ^{10}Be in pavement clasts atop bedrock mesas in the hyperarid Negev of Israel indicates that bedrock can protect pavements for as long as 305–331 ka on small bedrock mesas and for as long as 1.1 Ma for bedrock mesas with widths >60 m (Boroda et al., 2014). Basalt bedrock occurs under ancient pavements in the Great Basin (Zreda et al., 1993; Shepard et al., 1995; Heizler et al., 1999; Valentine and Harrington, 2006; Valentine et al., 2006) and Mojave (Shepard et al., 1995) deserts of the USA, as well as in the Canary Islands (Dunai and Wijbrans, 2000).

The case study of pavements on Salt and Verde terraces provide support for the importance of bedrock for pavement stability. The locations where we sampled the ~335 ka Sawik pavement (Fig. 8C) and the ~83 ka Mesa pavement (Fig. 8B) sit directly on strath terraces in the Sonoran Desert; granitic bedrock rests ~5 m underneath these pavement (Fig. 6C, F, I). In contrast, the Mesa terrace on the Verde River (Fig. 7C) and the Lousley Hills (Fig. 7F) terrace on the Verde River rest directly on playa clays. The age distribution of ^{10}Be dated clasts (Fig. 8E–F) show the greatest degree of variability – explained by the geomorphic instability of playa sediment.

The Stewart Mountain terrace gravels rest on top of fanglomerate (Fig. 5F). Quartzite clasts sampled atop the Stewart Mountain terrace (Fig. 6J-L) exhibit a distribution of ^{10}Be ages (Fig. 8D) with exposure ages centered at ~58 ka, ~80 ka, and ~110 ka. These ages are similar to other studies of pavements atop fanglomerate. A case study from the Mojave Desert alluvial fan points to pavements surviving until about 53–63 ka when the surface form of the alluvial fan begins to round (Oskin et al., 2007) due to ongoing gully incision. A maximum age for pavements on fanglomerate in Death Valley appears to be ~70 ka (Owen et al., 2011), while a Coachella Valley site could reach 260 ka (Matmon et al., 2006). Thus, for fanglomerate, ongoing erosion leads to clast exposure from beneath the pavement increasing the variability in cosmogenic ages (Frankel et al., 2007a).

4.7. Landform type

Landform type and setting may influence pavement stability. For example, flat wadi terraces are more stable than nearby alluvial fan pavements in the Libyan Desert (Adelsberger and Smith, 2009). The strath terraces of the Sawik and Mesa sites in the case study are the most stable in the Sonoran Desert. In the Precordillera of Argentina, alluvial fan pavements reach the end of their longevity after ~61 ka, but strath terraces can last to at least 181 ka (Hedrick et al., 2013). Placzek et al. (2014: 1503) note that bedrock, sediment on hillslopes, boulders on lower slopes and sediment in channels maintain different patterns of ^{10}Be accumulation in hyperarid, arid, and mesic climates. Table 6 includes the type of landform hosting desert pavements with reported ages around the globe, and ancient pavements are associated with basalt flows in arid regions (Wells et al., 1985; Shepard et al., 1995; Dunai and Wijbrans, 2000; Valentine and Harrington, 2006; Fenton and Niedermann, 2014) and with pediments in the Atacama Desert (Hall et al., 2008; Evenstar et al., 2009) and Australia (Fisher et al., 2014). A limitation of Table 6 is that cosmogenic nuclide studies only rarely focus on pavement antiquity. Pavements on top of landforms like alluvial fans (Nishiizumi et al., 2005; Wang et al., 2015) or alluvial plains (Matmon et al., 2009) provide an opportunity to generate minimum-limiting ages for the underlying form.

4.8. Clast size and shape

Reduction in clast size is associated with pavement stability in cold desert settings in Antarctica (Bockheim, 2010), in the hyperarid Negev (Matmon et al., 2009), in the hyperarid Sahara Desert (Adelsberger and Smith, 2009), basalt flows in semi-arid Nevada (Valentine et al., 2006), and in the Sonoran Desert (Huckleberry, 1993, 1994).

Unstable pavements on alluvial deposits can see an increase in clast size, as erosion can expose larger-sized clasts from alluvial-fan gravels (Frankel and Dolan, 2007). This is the case for sloping surfaces in north-central Chile (Rodriguez et al., 2013a), in the Cima volcanic field of the Mojave Desert (Wood et al., 2005) and the Libyan Plateau of Egypt (Adelsberger and Smith, 2009).

However, in the case study of the Salt and Verde terraces, the most stable Sawik and Mesa pavements are composed of quartzite alluvium with the original rounding from fluvial abrasion (Fig. 6B–F) that have not experienced clast-size reduction. The Sawik and Mesa terrace pavement cobbles have an oblong shape, many retaining their fluvially abraded and rounded edges. Because the short axis is much less than the long and intermediate axes, the cobbles have a flat shape.

Field experiments indicate that dust is trapped underneath pavement cobbles most efficiently when they are flattened and elongated (Goosens, 1995), and strontium isotope data from the oldest Sawik and Mesa terraces reveals that dust infiltrated down into the soil to depths of 50 cm (Fig. 11) – perhaps through process of moving down the fractures between peds (Anderson et al., 2002). Thus, while clast size reduction is generally important to pavement stability, it is not completely necessary – at least where clast shape works in tandem with dust trapping.

5. Conclusion

Ancient landforms hold value in Earth science, in part because they provide insight into the processes by which landscapes evolve. This is particularly true for desert pavements, where pavements are often a starting point for sorting out webs of complex age relationships. In some cases, pavements can provide key evidence for the timing of climatic transitions such as in Australia (Fujioka et al., 2005) or the southern Levant deserts (Amit et al., 2011). Old pavements compose a part of a complex Quaternary system of desert soils and desert biota (Peterson, 1981; Peterson et al., 1995; McFadden et al., 1998; Young et al., 2004; Wood et al., 2005). Many Earth scientists walking across old pavements

have seen abundant evidence of past occupants in the form of scattered stone tools or altered surfaces (Adelsberger and Smith, 2009; Latorre et al., 2013; Foley and M.M., 2015; Honegger and Williams, 2015). Thus, the general issue of pavement longevity connects to a variety of Earth science fields of study. This paper reviews scholarship on the evidence for and reasons for pavement longevity; then, this paper contextualizes prior scholarship through the lens of a case study of pavements along the terraces of the Salt and Verde Rivers, Sonoran Desert, Arizona, USA.

Just as alluvial fans have "personalities" in their behavior that vary with drainage basin characteristics of rock type, relief, drainage density, vegetation change, present-day climatology, paleoclimatology, land-use and more (Committee on Alluvial Fan Flooding, 1996), so do desert pavements. A unified theory of pavement longevity, unfortunately, cannot be extracted from our analysis of scholarship or from our study of pavements on terraces of the Salt and Verde Rivers. A great number of factors require consideration in understanding a desert pavement's geomorphic longevity or instability, and even the relative importance of these factors appear to shift from site to site. This concluding section of the paper attempts a general synthesis by grouping survival factors into three general categories: vital factors; key factors; and site-specific factors.

5.1. Vital factor in long-term pavement stability

Scholarship on pavements reveals one vital factor promoting pavement longevity: long-term hyperaridity that minimizes disturbance (Matmon et al., 2009). The oldest known pavements occur in regions that presently experience hyperaridity (Matmon et al., 2009; Placzek et al., 2014; Wang et al., 2015). Gypsum (and carbonate) precipitation may be a key mechanism of pavement survival related to hyperarid regions (Dunai et al., 2005; Clark, 2006; Evenstar et al., 2009; Matmon et al., 2009; Amit et al., 2011; Boroda et al., 2013; Wang et al., 2015). Clast-size reduction (Matmon et al., 2009) is also associated with long-term hyperaridity.

5.1.1. Key factors in Pleistocene pavement stability

Several key factors promote the survival of Pleistocene pavements for 10^4 to 10^5 years: allochthonous dust floating the pavement; flat topography; and a lack of headward-retreating swales or gullies.

1. Allochthonous dust floating pavement clasts. Dust infiltrating beneath desert pavements and keeping them at the surface – first recognized in Australia (Mabbutt, 1977; Mabbutt, 1979) and replicated globally (McFadden et al., 1986; Gerson and Amit, 1987; McFadden et al., 1987; Sauer et al., 2007; Adelsberger and Smith, 2009; Fisher et al., 2014; Wang et al., 2015) – can keep pavements alive and the lack thereof results in pavement instability. This is the case along the Salt and Verde Rivers where terrace pavements maintain their longevity as long as there exists a strontium-isotope signal indicating the presence of allochthonous dust (Fig. 11).
2. Flat topography. Sloping surfaces, with the exception of those in hyperarid regions (Boroda et al., 2013; Owen et al., 2013), promote pavement instability (Matmon et al., 2005; Wood et al., 2005; Adelsberger and Smith, 2009). In contrast, very low slope angles foster pavement stability (Cooke, 1970; Mabbutt, 1979; Dixon, 2009). This is the case for pavements on the Sawik, Mesa, and Blue Point terraces of the Salt River that maintain stability, while those with sloping surfaces experience ongoing exposure of alluvium eroding from underlying gravels.
3. Lack of headward retreating swales or gullies. Gully incision decreases pavement stability (Hunt and Mabey, 1966) with clear evidence found from cosmogenic nuclide data (Frankel et al., 2007a; Huang et al., 2014). Pavements atop isolated remnants of the Sawik (Fig. 5B) and Mesa (Fig. 5C) terrace of the Salt River exemplify pavement stability when swales or gullies do not work into an area of old desert pavement.

5.2. Site specific factors promoting pavement stability

Each pavement exists in a unique local setting with varying geology, landform, soils, hydrology, vegetation, climate, anthropogenic influences, and changes over time. As a consequence, it is inevitable that site-specific factors play important roles in pavement longevity. For example, the granitic strath underlying the Sawik and Mesa terrace pavements of the Salt River (Fig. 6F, I) promotes pavement stability over the much weaker playa clay strath of the Verde River (Fig. 7C, F). Similarly, the disk-shapes of the Salt River pavements (Fig. 6B, E, H, K) traps dust efficiently underneath this flattened shape (Goosens, 1995). Basalt flows in arid regions (Wells et al., 1985; Shepard et al., 1995; Dunai and Wijbrans, 2000; Valentine and Harrington, 2006; Fenton and Niedermann, 2014) provide a very stable substrate for pavements as the basalt gradually undergoes clast-size reduction (Valentine et al., 2006). In some places, deflation erodes pavements (Schmidt et al., 2011), while in other settings surface wash degrades pavement surfaces (Wood et al., 2005; Adelsberger and Smith, 2009; Rodriguez et al., 2013a). However, perhaps the best example of a site-specific factor would be modern and paleo-biotic disturbance (McAuliffe, 1994; Dickerson et al., 2013; Pietrasiak et al., 2014). By sampling pavements lacking evidence of modern or paleo-disturbance, exposure ages for Sawik pavement cobbles (Fig. 6G) reach ~332 ka (Table 7; Fig. 8C). It is the existence of these site-specific factors that makes development of a universal explanation for pavement stability most difficult.

Acknowledgements

We thank the late Troy Péwé for introducing the second author to the complexities of the Salt River terraces and for assisting in the collection of soil data on the Sawik, Mesa, and Blue Point terraces. The manuscript benefited greatly from the comments of the two anonymous reviewers and the editor. This research was supported by the Ministry of Education of the Republic of Korea and the National Research Foundation of Korea (NRF-2015S1A5A2A01010253 for Y.B. Seong) and by the Korea Polar Research Institute Grant PP16010.

References

Abrahams, A.D., Parsons, A.J., 1991. Relationship between infiltration and stone cover on a semiarid hillslopes, southern Arizona. J. Hydrol. 122, 49–59.
Abrahams, A.D., Parsons, A.J., 1994. Hydraulics of interrill overland flow on stone-covered desert surfaces. Catena 23, 111–140.
Abrahams, A.D., Soltyka, N., Parsons, A.J., Hirsch, P.J., 1990. Fabric analysis of a desert debris slope: Bell Mountain, California. J. Geol. 98, 264–272.
Adelsberger, K.A., Smith, J.R., 2009. Desert pavement development and landscape stability on the Eastern Libyan Plateau, Egypt. Geomorphology 107, 178–194.
Adelsberger, K.A., Smith, J.R., McPherron, S.P., Dibble, H.L., Olszewski, D.I., Schurmans, U.A., Chiotti, L., 2013. Desert pavement disturbance and artifact taphonomy: a case study from the Eastern Libyan Plateau, Egypt. Geoarchaeology 28, 112–130.
Aerts, R., Finneran, N., Mitiku, H., Poesen, J., 2010. The accumulation of Stone Age lithic artifacts in rock fragment mulches in northern Ethiopia. Geoarchaeology 25, 137–148.
Al-Farraj, A., 2008. Desert pavement development on the lake shorelines of Lake Eyre (South), South Australia. Geomorphology 100, 154–163.
Al-Farraj, A., Harvey, A.M., 2000. Desert pavement characteristics on Wadi terrace and alluvial fan surfaces: Wadi Al-Bih, UAE. Geomorphology 35, 279–297.
Amit, R., Gerson, R., 1986. The evolution of Holocene reg (gravelly) soils in deserts - and example from the Dead Sea region. Catena 13, 59–79.
Amit, R., Gerson, R., Yaalon, D.H., 1993. Stages and rate of the gravel shattering process by salts in desert reg soils. Geoderma 57, 295–324.
Amit, R., Enzel, Y., Grodek, T., Crouvi, O., Porat, N., Ayalon, A., 2010. The role of rare rainstorms in the formation of calcic soil horizons on alluvial surfaces in extreme deserts. Quat. Res. 74, 177–187.
Amit, R., Simhai, O., Ayalon, A., Enzel, Y., Matmon, A., Crouvi, O., Porat, N., McDonald, E., 2011. Transition from arid to hyper-arid environment in the southern Levant deserts as recorded by early Pleistocene cumulic Aridisols. Quat. Sci. Rev. 30, 312–313.
Amundson, R., Dietrich, W., Bellugi, D., Ewing, S., Nishiizumi, K., Chong, G., Owen, J., Finkel, R., Heimsath, A., Stewart, B., 2012. Geomorphologic evidence for the late Pliocene onset of hyperaridity in the Atacama Desert. Geol. Soc. Am. Bull. 124, 1048–1070.
Anders, M.D., Pederson, J.L., Rittenour, T.M., Sharp, W.D., Gosse, J.C., Karlstrom, K.E., Crossey, L.J., Goble, R.J., Stockli, L., Yang, G., 2005. Pleistocene geomorphology and geochronology of eastern Grand Canyon: linkages of landscape components during climate changes. Quat. Sci. Rev. 24, 2428–2448.

Anderson, R.S., Repka, J.L., Dick, G.S., 1996. Explicit treatment of inheritance in dating depositional surfaces using in situ ^{10}Be and ^{26}Al. Geology 24, 47–51.

Anderson, K., Wells, S., Graham, R., 2002. Pedogenesis of vesicular horizons, Cima Volcanic Field, Mojave Desert, California. Soil Sci. Soc. Am. J. 66, 878–887.

Armstrong, P.A., Perez, R., Owen, L.A., Finkel, R.C., 2010. Timing and controls on late Quaternary landscape development along the eastern Sierra El Mayor range front in northern Baja California, Mexico. Geomorphology 114, 415–430.

Athanassas, C.D., Rollefson, G.O., Kadereit, A., Kennedy, D., Theodorakopoulou, K., Rowan, Y.M., Wasse, A., 2015. Optically stimulated luminescence (OSL) dating and spatial analysis of geometric lines in the Northern Arabian Desert. J. Archaeol. Sci. 64, 1–11.

Baied, C.A., Somonte, C., 2013. Mid-Holocene geochronology, palaeoenvironments, and occupational dynamics at Quebrada de Amaicha, Tucuman, Argentina. Quat. Int. 299, 80–89.

Balco, G., Stone, J.O., Lifton, N.A., Dunai, T.J., 2008. A complete and easily accessible means of calculating surface exposure ages or erosion rates from ^{10}Be and ^{26}Al measurements. Quat. Geochronol. 3, 174–195.

Balco, G., Briner, J., Finkel, R.C., Rayburn, J.A., Ridge, J.C., Schaefer, J.M., 2009. Regional beryllium-10 production rate calibration for late-glacial northeastern North America. Quat. Geochronol. 4, 93–107.

Benson, L.V., al, e., 1990. Chronology of expansion and contraction of four Great Basin lake systems during the past 35,000 years. Palaeogeogr. Palaeoclimatol. Palaeoecol. 78, 241–286.

Blisniuk, K., Rockwell, T., Owen, L.A., Oskin, M., Lippincott, C., Caffee, M.W., Dortch, J., 2010. Late Quaternary slip rate gradient defined using high-resolution topography and ^{10}Be dating of offset landforms on the southern San Jacinto Fault zone, California. J. Geophys. Res. Solid Earth 115. http://dx.doi.org/10.1029/2009JB006346.

Blisniuk, K., Oskin, M., Fletcher, K., Rockwell, T., Sharp, W., 2012. Assessing the reliability of U-series and ^{10}Be dating techniques on alluvial fans in the Anza Borrego Desert, California. Quat. Geochronol. 13, 26–41.

Bockheim, J.G., 2010. Evolution of desert pavements and the vesicular layer in soils of the Transantarctic Mountains. Geomorphology 118, 433–443.

Boroda, R., Amit, R., Matmon, A., ASTERTeam, Finkel, R., Porat, N., Enzel, Y., Eyal, Y., 2011. Quaternary-scale evolution of sequences of talus flatirons in the hyperarid Negev. Geomorphology 127, 41–52.

Boroda, R., Matmon, A., Amit, R., Haviv, I., Porat, N., ASTERTeam, Rood, D., Eyal, Y., 2013. Long-term talus flatirons formation in the hyperarid northeastern Negev, Israel. Quat. Res. 79, 256–267.

Boroda, R., Matmon, A., Amit, R., Haviv, I., Arnold, M., Aumaître, G., Bourles, D.L., Keddadouche, K., Eyal, Y., Enzel, Y., 2014. Evolution and degradation of flat-top mesas in the hyper-arid Negev, Israel revealed from ^{10}Be cosmogenic nuclides. Earth Surf. Process. Landf. 39, 1611–1621.

Borrazzo, K., Lithic taphonomy in desert environments: contributions from Fuego-Patagonia (Southern South America). Quat. Int. http://dx.doi.org/10.1016/j.quaint.2015.12.012 (in press).

Brazel, A.J., 1989. Dust and climate in the American Southwest. In: Leinen, M. (Ed.), Paleoclimatology and Paleometeorology: Modern and Past Patterns of Global Atmospheric Transport. Kluwer Academic Publishers, Dordrecht, pp. 65–96.

Breed, C.S., McCauley, J.F., Whitney, M.I., 1989. Wind erosion forms. In: Thomas, D. (Ed.), Arid Zone Geomorphology. Belhaven Press, London, pp. 284–307.

Brookes, I.A., 1993. Geomorphology and Quaternary geology of the Dakhla Oasis Region, Egypt. Quat. Sci. Rev. 12, 529–552.

Brookes, I.A., 2001. Aeolian erosional lineations in the Libyan Desert, Dahkla Region, Egypt. Geomorphology 39, 189–209.

Bubenzer, O., Besler, H., Hilgers, A., 2007. Filling the gap: OSL data expanding 14C chronologies of Late Quaternary environmental change in the Libyan Desert. Quat. Int. 175, 41–52.

Campbell, S.W., 1999. Aspects of landscape evolution in arid environments (M.S. Thesis) Geography. University of Arkansas, Fayetteville, pp. 1–57.

Capo, R.C., Stewart, B.W., Chadwick, O.A., 1998. Strontium isotopes as tracers of ecosystem processes: theory and methods. Geoderma 82, 197–225.

Capo, R.C., Chadwick, O.A., 1999. Sources of strontium and calcium in desert soil and calcrete. Earth Planet. Sci. Lett. 170, 61–72.

Cerveny, N.V., Kaldenberg, R., Reed, J., Whitley, D.S., Simon, J., Dorn, R.I., 2006. A new strategy for analyzing the chronometry of constructed rock features in deserts. Geoarchaeology 21, 181–203.

Chmeleff, J., von Blanckenburg, F., Kossert, K., Jakob, D., 2010. Determination of the ^{10}Be half-life by multicollector ICP-MS and liquid scintillation counting. Nucl. Instrum. Methods Phys. Res., Sect. B 268, 192–199.

Choi, J.H., Murray, A.S., Jain, M., Cheong, C.S., Chang, H.W., 2003. Luminescence dating of well-sorted marine terrace sediments on the southeastern coast of Korea. Quat. Sci. Rev. 22, 407–421.

Clark, J.D.A., 2006. Antiquity of aridity in the Chilean Atacama Desert. Geomorphology 73, 101–114.

Colinvaux, P.A., DeOliveira, P.E., Bush, M.B., 2000. Amazonian and neotropical plant communities on glacial time-scales: the failure of the aridity and refuge hypotheses. Quat. Sci. Rev. 19, 141–169.

Committee on Alluvial Fan Flooding, N.R.C., 1996. Alluvial Fan Flooding. National Academy of Science Press, Washington D.C. (172 pp.).

Cook, J.P., Pearthree, P.A., Onken, J.A., Youberg, A., Bigio, E.R., 2010. Mapping of the Holocene River Alluvium Along the Verde River, Central Arizona. Report to the Adjudication and Technical Support Unit Surface Water Division Arizona Department of Water Resources. 10 Sheets Map Scale 1:24,000. Arizona Geological Survey, Tucson (51 pp.).

Cooke, R.U., 1970. Stone pavements in deserts. Ann. Assoc. Am. Geogr. 60, 560–577.

Cooke, R.U., Warren, A., 1973. Geomorphology in Deserts. University of California Press, Berkeley (374 pp.).

Cortes, A., González, L., Binnie, S.A., Robinson, R., Freeman, S.P.H.T., Vargas, E., (2). 2012. Paleoseismology of the Mejillones Fault, northern Chile: insights from cosmogenic ^{10}Be and optically stimulated luminescence determinations. Tectonics 31, http://dx.doi.org/10.1029/2011TC002877.

Cremaschi, M., Zerboni, A., Mercuri, A.M., Olmi, L., Biagetti, S., de Lernia, S., 2014. Takarkori rock shelter (SW Libya): an archive of Holocene climate and environmental changes in the central Sahara. Quat. Sci. Rev. 101, 36–60.

Cyr, A.J., Miller, D.M., Reheis, M.C., Mahan, S.A., Stock, J.D., Schmidt, K.M., 2010. Climatically driven changes in erosion rates recorded in alluvial fan sediments, Providence Mountains, eastern Mojave Desert, California. AGU Fall Meeting Abstracts 1, p. 0712.

Cyr, A.J., Miller, D.M., Mahan, S.A., 2015. Paleodischarge of the Mojave River, southwestern United States, investigated with single-pebble measurements of 10Be. Geosphere 11, 1158–1171.

Dan, J., Yaalon, D.H., Moshe, R., Nissim, S., 1982. Evolution of reg soils in southern Israel and Sinai. Geoderma 28, 173–202.

deHaas, T., Ventra, D., Carbonneau, P.E., Kleinhans, M.G., 2014. Debris-flow dominance of alluvial fans masked by runoff reworking and weathering. Geomorphology 217, 165–181.

Denny, C.S., 1965. Alluvial fans in the Death Valley region of California and Nevada. U.S. Geol. Surv. Prof. Pap. 466.

Denny, C.S., 1967. Fans and pediments. Am. J. Sci. 265, 81–105.

Dickerson, R.P., Cocks, G., 2015. Alluvial fan surfaces and an age-related stability for cultural resource preservation: Nevada Test and Training Range, Nellis Air Force Base, Nevada, USA. J. Archaeol. Sci. Rep. 2, 551–568.

Dickerson, R.P., Forman, A., Liu, T., 2013. Co-development of alluvial fan surfaces and arid botanical communities, Stonewall Flat, Nevada, USA. Earth Surf. Process. Landf. 38, 1083–1101.

Dietze, M., Kleber, A., 2012. Contribution of lateral processes to stone pavement formation in deserts inferred from clast orientation patterns. Geomorphology 139, 172–187.

Dietze, M., Muhs, S., Dietze, E., 2011. Ambiguities of relative age indicators on abandoned surfaces of arid environments. Z. Geomorphol. 55, 49–75.

Dietze, M., Bartel, S., Lindner, M., Kleber, A., 2012. Formation mechanisms and control factors of vesicular soil structure. Catena 99, 83–96.

Dietze, M., Groth, J., Kleber, A., 2013. Alignment of stone-pavement clasts by unconcentrated overland flow – implications of numerical and physical modelling. Earth Surf. Process. Landf. 38, 1234–1243.

Dietze, M., Dietze, E., Lomax, J., Fuchs, M., Kleber, A., Wells, S.G., 2016. Environmental history recorded in aeolian deposits under stone pavements, Mojave Desert, USA. Quat. Res. 85, 4–16.

Dixon, J.C., 1994. Aridic soils, patterned ground, and desert pavements. In: Abrahams, A.D., Parsons, A.J. (Eds.), Geomorphology of Desert Environments. Chapman, London, pp. 64–81.

Dixon, J.C., 2009. Aridic soils, patterned ground, and desert pavements. In: Parsons, A.J., Abrahams, A.D. (Eds.), Geomorphology of Desert Environments, 2nd ed. Springer, Amsterdam, pp. 101–122.

Donahue, D.J., LInick, T.W., Jull, A.J.T., 1990. Isotope-ratio and background corrections for accelerator mass spectrometry radiocarbon measurements. Radiocarbon 32, 135–140.

Dorn, R.I., 1986. Rock varnish as an indicator of aeolian environmental change. In: Nickling, W.G. (Ed.), Aeolian Geomorphology. Allen & Unwin, London, pp. 291–307.

Dorn, R.I., Dickinson, W.R., 1989. First paleoenvironmental interpretation of a pre-Quaternary rock varnish site, Davidson Canyon, south Arizona. Geology 17, 1029–1031.

Dorn, R.I., Oberlander, T.M., 1982. Rock varnish. Prog. Phys. Geogr. 6, 317–367.

Dortch, J., Schoenbohm, L.M., 2011. Multiple nuclide cosmogenic dating of very old desert pavements on the Puna Plateau, Northwest Argentina. AGU Fall Meeting Abstracts 1, p. 0605.

Duhnforth, M., Ivy-Ochs, S., Densmore, A.L., Kubik, P.W., 2007. Constraints on the timing of fan deposition in Death Valley, California, using cosmogenic ^{10}Be and ^{26}Al. Geol. Soc. Am. Abstr. Programs 39 (6), 260.

Dunai, T.J., Wijbrans, J.R., 2000. Long-term cosmogenic ^{3}He production rates (152 ka–1.35 Ma) from ^{40}Ar/^{39}Ar dated basalt flows at 29 N latitude. Earth Planet. Sci. Lett. 176, 147–156.

Dunai, T.J., Gonzalez-Lopez, G.A., Juez-Larre, J., 2005. Oligocene–Miocene age of aridity in the Atacama Desert revealed by exposure dating of erosion-sensitive landforms. Geology 33, 321–324.

Evenari, M., Yaalong, D.J., Gutterman, Y., 1974. Note on soils with vesicular structures in deserts. Z. Geomorphol. 18, 162–172.

Evenstar, L.A., Hartley, A.J., Stuart, F.M., Mather, A.E., Rice, C.M., Chong, G., 2009. Multiphase development of the Atacama Planation Surface recorded by cosmogenic ^{3}He exposure ages: implications for uplift and Cenozoic climate change in western South America. Geology 37, 27–30.

Ewing, S.A., Sutter, B., Owen, J., Nishiizumi, K., Sharp, W., Cliff, S.S., Perry, K., Dietrich, W., McKay, C.P., Amundson, R., 2006. A threshold in soil formation at Earth's arid–hyperarid transition. Geochim. Cosmochim. Acta 70, 5293–5322.

Fenton, C.R., Niedermann, S., 2014. Surface exposure dating of young basalts (1–200 ka) in the San Francisco volcanic field (Arizona, USA) using cosmogenic ^{3}He and ^{21}Ne. Quat. Geochronol. 19, 87e105.

Fenton, C.R., Pelletier, J.D., 2013. Cosmogenic ^{3}He age estimates of Plio-Pleistocene alluvial-fan surfaces in the Lower Colorado River Corridor, Arizona, USA. Quat. Res. 79, 86–99.

Fenton, C.R., Webb, R.H., Cerling, T.E., Poreda, R.J., Nash, B.P., 2002. Cosmogenic ^{3}He ages and geo-chemical discrimination of lava-dam outburst-flood deposits in western Grand Canyon, Arizona. In: House, P.K., Webb, R.h., Baker, V.R., Levish, D.R. (Eds.), Ancient Floods and Modern Hazards: Principles and Applications of Paleoflood Hydrology. American Geophysical Union, Washington D.C., pp. 191–215.

Fenton, C.R., Poreda, R.J., Nash, B.P., Webb, R.H., Cerling, T.E., 2004. Geochemical discrimination of five Pleistocene lava-dam outburst-flood deposits, Western Grand Canyon, Arizona. J. Geol. 112, 91–110.

Field, J.J., Pearthree, P.A., 1997. Geomorphologic flood-hazard assessment of alluvial fans and piedmonts. J. Geosci. Educ. 45, 27–37.

Field, J.H., Dodson, J.R., Prosser, I.P., 2002. A late Pleistocene vegetation history from the Australian semi-arid zone. Quat. Sci. Rev. 21, 1023–1037.

Fisher, A., Fink, D., Chappell, J., Melville, M., 2014. $^{26}Al/^{10}Be$ dating of an aeolian dust mantle soil in western New South Wales, Australia. Geomorphology 219, 201–212.

Fitzsimmons, K.E., Cohen, T.J., Hesse, P.P., Jansen, J., Nanson, G.C., May, J.H., Barrows, T.T., Harberla, D., Hilgers, A., Kelly, T., Larsen, J., Lomax, J., Treble, P., 2013. Late Quaternary palaeoenvironmental change in the Australian drylands. Quat. Sci. Rev. 74, 78–96.

Foley, R.A., M.M., L., 2015. Lithic landscapes: early human impact from stone tool production on the central Saharan environment. PLoS One 10 (3), e0116482 (doi:10.1371).

Frankel, K.L., Dolan, J.F., 2007. Characterizing arid region alluvial fan surface roughness with airborne laser swath mapping digital topographic data. J. Geophys. Res. 112. http://dx.doi.org/10.1029/2006JF000644.

Frankel, K.L., Brantley, K.S., Dolan, J.F., Finkel, R.C., Klinger, R.E., Knott, J.R., Machette, M.N., Owen, L.A., Phillips, F.M., Slate, J.L., Wernicke, B., 2007a. Cosmogenic ^{10}Be and ^{36}Cl geochronology of offset alluvial fans along the northern Death Valley fault zone: implications for transient strain in the eastern California shear zone. J. Geophys. Res. Solid Earth 112. http://dx.doi.org/10.1029/2006JB004350.

Frankel, K.L., Dolan, J.F., Finkel, R.C., Owen, L.A., Hoeft, J.S., 2007b. Spatial variations in slip rate along the Death Valley-Fish Lake Valley fault system determined from LiDAR topographic data and cosmogenic ^{10}Be geochronology. Geophys. Res. Lett. 34. http://dx.doi.org/10.1029/2007GL030549.

Frink, D.S., Dorn, R.I., 2001. Beyond taphonomy: Pedogenic transformations of the archaeological record in monumental earthworks. Ariz.-Nev. Acad. Sci. J. 34, 24–44.

Fuchs, M., Dietze, M., Al-Qudah, K., Lomax, J., 2015. Dating desert pavements: first results from a challenging environmental archive. Quat. Geochronol. 30, 342–349. http://dx.doi.org/10.1016/j.quageo.2015.01.001 (in press).

Fujioka, T., Chappell, J., Honda, M., Yatsevich, I., Fifield, L.K., Fabel, D., 2005. Global cooling initiated stony deserts in central Australia 2–4 Ma, dated by cosmogenic ^{21}Ne–^{10}Be. Geology 33, 993–996.

Fukioka, T., Chappell, J., 2011. Desert landscape processes on a timescale of millions of years, probed by cosmogenic nuclides. Aeolian Res. 3, 157–164.

Gerson, R., Amit, R., 1987. Rates and modes of dust accretion and deposition in an arid region – the Negev, Israel. J. Geol. Soc. Lond. Spec. Publ. 35, 157–169.

Gile, L.H., Hawley, J.W., Grossman, R.B., 1981. Soils and geomorphology in the Basin and Range area of southern New Mexico. Guidebook to the Desert Project. New Mexico Bureau of Mines and Mineral Resources Memoir 39, pp. 1–222.

Goehring, B.M., Schimmelpfennig, I., Schaefer, J.M., 2014. Capabilities of the Lamont–Doherty Earth Observatory in situ ^{14}C extraction laboratory updated. Quat. Geochronol. 19, 194–197.

Goethals, M.M., Niedermann, S., Hetzel, R., Fenton, C.R., 2007. Cosmogenic nuclide intercalibration and erosion rate study on fault scarps of the Bishop Tuff, CA, USA. Geochim. Cosmochim. Acta 71 (15), A335.

Gonzalez, G., Dunai, T., Carrizo, D., Allmendinger, R., 2006. Young displacements on the Atacama Fault System, northern Chile from field observations and cosmogenic ^{21}Ne concentrations. Tectonics 25, TC3006. http://dx.doi.org/10.1029/2005TC001846.

Goosens, D., 1995. Field experiments of aeolian dust accumulation on rock fragment substrata. Sedimentology 42, 391–402.

Goudie, A., Wilkinson, J., 1977. The Warm Desert Environment. Cambridge University Press, Cambridge (88 pp.).

Graham, R.C., Hirmas, D.R., Wood, Y.A., Amrhein, C., 2008. Large near-surface nitrate pools in soils capped by desert pavement in the Mojave Desert, California. Geology 36, 259–262.

Granger, D.E., 2006. A review of burial dating methods using ^{26}Al and ^{10}Be. In: Siame, L., Bourles, D., Brown, E.T. (Eds.), In-situ-produced Cosmogenic Nuclides and Quantification of Geological ProcessesGeological Society of America Special Paper 415. Geological Society of America, Boulder, pp. 1–16.

Gray, H.J., Owen, L.A., Dietsch, C., Beck, R.A., Caffee, M.A., Finkel, R.C., Mahan, S.A., 2014. Quaternary landscape development, alluvial fan chronology and erosion of the Mecca Hills at the southern end of the San Andreas Fault zone. Quat. Sci. Rev. 105, 66–85.

Grolier, M.J., Ericksen, G.E., McCauley, J.F., Morris, E.C., 1974. The desert land forms of Peru; a preliminary photographic atlas. U.S. Geological Survey Open File Report, pp. 74–1044 (http://pubs.er.usgs.gov/publication/ofr741044).

Guralnik, B., Matmon, A., Avni, Y., Fink, D., 2010. ^{10}Be exposure ages of ancient desert pavements reveal Quaternary evolution of the Dead Sea drainage basin and rift margin tilting. Earth Planet. Sci. Lett. 290, 132–141.

Guralnik, B., Matmon, A., Avni, Y., Porat, N., Fink, D., 2011. Constraining the evolution of river terraces with integrated OSL and cosmogenic nuclide data. Quat. Geochronol. 6, 22–32.

Haff, P.K., 2001. Desert pavement: an environmental canary? J. Geol. 109, 661–668.

Haff, P.L., 2005. Response of desert pavement to seismic shaking, Hector Mine earthquake, California, 1999. J. Geophys. Res. Earth Surf. 110. http://dx.doi.org/10.1029/2003JF000054.

Haff, P.K., 2014. Biolevitation of pebbles on desert surfaces. Granul. Matter 16, 275–278.

Hall, S.R., Farber, D.L., Audin, L., Finkel, R., Mériaux, A., 2008. Geochronology of pediment surfaces in southern Peru: implications for Quaternary deformation of the Andean forearc. Tectonophysics 429, 186–205.

Hayden, J., 1976. Pre-altithermal archaeology in the Sierra Pinacate, Sonora, Mexico. Am. Antiq. 41, 274–289.

Hedrick, K., Owen, L.A., Rockwell, T.K., Meigs, A., Costa, C., Caffee, M.W., Masana, E., Ahumada, E., 2013. Timing and nature of alluvial fan and strath terrace formation in the Eastern Precordillera of Argentina. Quat. Sci. Rev. 80, 143–168.

Heimsath, A.M., Chappell, J., Dietrich, W.E., Nishiizumi, K., Finkel, R., 2001. Late Quaternary erosion in southeastern Australia: a field example using cosmogenic nuclides. Quat. Int. 83-85, 169–185.

Heisinger, B., Lal, D., Kubik, P., Ivy-Ochs, S., Knie, K., Nolte, E., 2002a. Production of selected cosmogenic radionuclides by muons: 2. Capture of negative muons. Earth Planet. Sci. Lett. 200, 357–369.

Heisinger, B., Lal, D., Kubik, P., Ivy-Ochs, S., Neumaier, S., Knie, K., Lazarev, V., Nolte, E., 2002b. Production of selected cosmogenic radionuclides by muons: 1. Fast muons. Earth Planet. Sci. Lett. 200, 345–355.

Heizler, M.T., Perry, F.V., Crowe, B.M., Peters, L., Appelt, R., 1999. The age of Lathrop Wells volcanic center: an $^{40}Ar/^{39}Ar$ dating investigation. J. Geophys. Res. Solid Earth 104 (*B*1), 767–804.

Hetz, G., Mushkin, A., Blumberg, D.G., Baer, G., Ginat, H., 2016. Estimating the age of desert alluvial surfaces with spaceborne radar data. Remote Sens. Environ. 184, 288–301.

Hetzel, R., Tao, M., Stokes, S., Niedermann, S., Ivy-Ochs, S., Gao, B., Strecker, M.R., Kubik, P.W., 2004. Late Pleistocene/Holocene slip rate of the Zhangye thrust (Qilian Shan, China) and implications for the active growth of the northeastern Tibetan Plateau. Tectonics 23, TC6006.

Hidy, A.J., Gosse, J.C., Pederson, J.L., Mattern, J.P., Finkel, R.C., 2010. A geologically constrained Monte Carlo approach to modeling exposure ages from profiles of cosmogenic nuclides: an example from Lees Ferry, Arizona. G3 Geochem. Geophys. Geosyst. 11. http://dx.doi.org/10.1029/2010GC003084.

Hippe, K., Kober, F., Baur, H., Ruff, M., Wacker, L., Wieler, R., 2009. The current performance of the in situ ^{14}C extraction line at ETH. Quat. Geochronol. 4, 493–500.

Hippe, K., Kober, F., Wacker, L., Fahrni, S.M., Ivy-Ochs, S., Akçar, N., Schluchter, C., Wieler, R., 2013. An update on in situ cosmogenic ^{14}C analysis at ETH Zurich. Nucl. Instrum. Methods Phys. Res., Sect. B 294, 81–86.

Honegger, M., Williams, M., 2015. Human occupations and environmental changes in the Nile valley during the Holocene: the case of Kerma in Upper Nubia (northern Sudan). Quat. Sci. Rev. 130, 141–154.

Honker, A.M., 2002. A River Sometimes Runs Through It: A History of Salt River Flooding and Phoenix (Ph.D. Dissertation) Arizona State University, Tempe (294 pp.).

Huang, W.L., Yang, X.P., Li, A., THompson, J.A., Zhang, L., 2014. Climatically controlled formation of river terraces in a tectonically active region along the southern piedmont of the Tian Shan, NW China. Geomorphology 220, 15–29.

Huckleberry, G., 1993. Surficial geology of the Middle Gila River Area, North-Central Pinal County, Arizona. Arizona Geological Survey Open File Report 93-3, pp. 1–52.

Huckleberry, G., 1994. Surficial geology of the Santan Mountains Piedmont Area, Northern Pinal and Eastern Maricopa County Area, Arizona. Arizona Geological Survey Open-File Rpoert 94-7, pp. 1–32.

Hunt, A., 1960. Archaeology of the Death Valley salt pan. University of Utah Archaeological Paper No. 47.

Hunt, C.B., Mabey, D.R., 1966. Stratigraphy and structure, Death Valley, California. U.S. Geol. Surv. Prof. Pap. 494A.

Hussain, S.H., Aghwan, T.A., 2014. Sedimentology and evolution of a foreland desert basin, Middle Eocene Gercus Formation (North and Northeastern Iraq). Arab. J. Geosci. 8, 2799–2830.

Ivy-Ochs, S., Dühnforth, M., Densmore, A.L., Alfimov, V., 2013. Dating fan deposits with cosmogenic nuclides. In: Schneuwly-Bollschweiler, M., Stoffel, M., Florian., R.-M. (Eds.), Dating Torrential Processes on Fans and Cones. Springer, Amsterdam, pp. 243–263.

Jessup, R.W., 1951. The soils, geology, and vegetation of northwestern South Australia. R. Soc. S. Aust. Trans. 74, 189–273.

Jessup, R.W., 1960. The stony tableland soils of the southeastern portion of the Australian arid zone and their evolutionary history. J. Soil Sci. 11, 188–196.

Jianjun, Q., Ning, H., Guangrong, D., Weimin, Z., 2001. The role and significance of the Gobi Desert pavement in controlling sand movement on the cliff top near the Dunhuang Magao Grottoes. J. Arid Environ. 48, 357–371.

Johnson, D.L., 1989. Subsurface stone lines, stone zones, artifact-manuport layers, and biomantles produced by bioturbation via pocket gophers (*Thomomys bottae*). Am. Antiq. 54, 370–389.

Johnson, D.L., 1990. Biomantle evolution and the redistribution of earth materials and artifacts. Soil Sci. 149, 84–102.

Johnson, D.L., Balek, C.L., 1991. The genesis of Quaternary landscapes with stone lines. Phys. Geogr. 12, 3855–3895.

Jungers, M.C., Heimsath, A.M., Amundson, R., Balco, G., Shuster, D., Cong, G., 2013. Active erosion–deposition cycles in the hyperarid Atacama Desert of Northern Chile. Earth Planet. Sci. Lett. 371-372, 125–133.

Kianian, M.K., 2014. Studying surface properties of pavements and their relation to soil properties and plant growth in Hajaligholi playa, Iran. Arab. J. Geosci. 7, 1457–1461.

Kim, D.E., Seong, Y.B., Byun, J.M., Weber, J., Min, K., 2016. Geomorphic disequilibrium in the Eastern Korean Peninsula: possible evidence for reactivation of a rift-flank margin? Geomorphology 254, 130–145.

Kohl, C.P., Nishiizumi, K., 1992. Chemical isolation of quartz for measurement of in-situ produced cosmogenic nuclides. Geoch. Cosmoch. Acta 56, 3583–3587.

Korschinek, G., Bergmaier, A., Faestermann, T., Gerstmann, U.C., Knie, K., Rugel, G., Wallner, A., Dillmann, I., Dollinger, G., Lierse von Gostomski, C., Kossert, K., Maiti, M., Poutivtsev, M., Remmert, A., 2010. A new value for the half-life of ^{10}Be by heavy-ion elastic recoil detection and liquid scintillation counting. Nucl. Instrum. Methods Phys. Res., Sect. B 268, 187–191.

Kring, D.A., McHargue, L.R., Bland, P.A., Hill, D.H., Berry, F.J., 2001. Gold Basin meteorite strewn field, Mojave Desert, northwestern Arizona: relic of a small late Pleistocene impact event. Meteorit. Planet. Sci. 36, 1057–1066.

Ku, T.L., Bull, W.B., Freeman, S.T., Knauss, K.G., 1979. Th-230/U-234 dating of pedogenic carbonates in gravelly desert soils of Vidal Valley, southeastern California. Geol. Soc. Am. Bull. 90, 1063–1073.
Laity, J.E., 2011. Pavements and stony mantles. In: Thomas, D.S.G. (Ed.), Arid Zone Geomorphology, 3rd edition Wiley, London, pp. 181–207.
Lal, D., 1991. Cosmic ray labeling of erosion surfaces: in situ nuclide production rates and erosion models. Earth Planet. Sci. Lett. 104, 424–439.
Larson, P.H., Dorn, R.I., Douglass, J., Gootee, B.F., Arrowsmith, R., 2010. Stewart Mountain Terrace: a new Salt River terrace with implications for landscape evolution of the lower Salt River Valley, Arizona. J. Ariz. Nev. Acad. Sci. 42, 26–36.
Larson, P.H., Kelley, S.B., Dorn, R.I., Seong, Y.B., 2017. Pediment development and the pace of landscape change in the northeastern Sonoran Desert, United States. Ann. Assoc. Am. Geogr. (http://www.tandfonline.com/doi/full/10.1080/24694452.2016.1201420).
Latorre, C., Santoro, C.M., Ugalde, P.C., Gayo, E.M., Osorio, D., Salas-Egana, C., Pol-Holz, R., Joly, D., Rech, J.A., 2013. Late Pleistocene human occupation of the hyperarid core in the Atacama Desert, northern Chile. Quat. Sci. Rev. 77, 19–30.
Lebedeva, M.P., Golovanov, D.L., Abrosimov, K.N., 2016. Micromorphological diagnostics of pedogenetic, eolian, and colluvial processes from data on the fabrics of crusty horizons in differently aged extremely aridic soils of Mongolia. Quat. Int. (in press).
LeBeon, M., Klinger, Y., Al-Qaryouti, M., Meriaux, A.S., Finkel, R.C., Elias, A., Mayyas, O., Ryerson, F.J., Tapponnier, P., 2010. Early Holocene and Late Pleistocene slip rates of the southern Dead Sea Fault determined from ^{10}Be cosmogenic dating of offset alluvial deposits. J. Geophys. Res. Solid Earth 115. http://dx.doi.org/10.1029/2009JB007198.
Lifton, N.A., Jull, T., Quade, J., 2001. A new extraction technique and production rate estimate for in situ cosmogenic ^{14}C in quartz. Geochim. Cosmochim. Acta 65, 1953–1969.
Liu, T., 2016. VML dating lab. http://www.vmldating.com/ (last accessed March 13).
Liu, T., Broecker, W.S., 2007. Holocene rock varnish microstratigraphy and its chronometric application in drylands of western USA. Geomorphology 84, 1–21.
Liu, T., Broecker, W.S., 2008a. Rock varnish evidence for latest Pleistocene millennial-scale wet events in the drylands of western United States. Geology 36, 403–406.
Liu, T., Broecker, W.S., 2008b. Rock varnish microlamination dating of late Quaternary geomorphic features in the drylands of the western USA. Geomorphology 93, 501–523.
Liu, T., Broecker, W.S., 2013. Millennial-scale varnish microlamination dating of late Pleistocene geomorphic features in the drylands of western USA. Geomorphology 187, 38–60.
Liu, T., Broecker, W., Stein, M., 2013. Rock varnish evidence for a Younger Dryas wet event in the Dead Sea basin. Geophys. Res. Lett. 40, 2229–2235.
Lv, Y., Gu, Z., Aldahan, A., Zhang, H., Possnert, G., Lei, G., 2010. ^{10}Be in quartz gravel from the Gobi Desert and evolutionary history of alluvial sedimentation in the Ejina Basin, Inner Mongolia, China. Chin. Sci. Bull. 55, 3802–3809.
Mabbutt, J.A., 1965. Stone distribution in a stony tablel and soil. Aust. J. Soil Res. 3, 131–142.
Mabbutt, J.C., 1977. Desert Landforms. Australian National University Press, Canberra (340 pp.).
Mabbutt, J.A., 1979. Pavements and patterned ground in the Australian stony deserts. Stuttg. Geogr. Stud. 93, 107–123.
Machette, M.N., Slate, J.L., Phillips, F.M., 2008. Terrestrial cosmogenic-nuclide dating of alluvial fans in Death Valley, California. U.S. Geol. Surv. Prof. Pap. 1755, 1–44.
Marchant, D.R., Denton, G.H., 1996. Miocene and Pliocene paleoclimate of the Dry Valleys region, Southern Victoria land: a geomorphological approach. Mar. Micropaleontol. 27, 253–271.
Marchant, D.R., Schisher, C., Lux, D., West, D., Denton, G., 1993. Pliocene paleoclimate and East Antarctic ice-sheet history from surficial ash deposits. Science 260, 667–670.
Marchant, D.R., Denton, G.H., Swisher, C.C., Potter, N., 1996. Late Cenozoic Antarctic paleoclimate reconstructed from volcanic ashes in the Dry Valleys region of southern Victoria Land. Geol. Soc. Am. Bull. 108, 181–194.
Marchetti, D.W., Cerling, T.E., 2005. Cosmogenic ^{3}He exposure ages of Pleistocene debris flows and desert pavements in Capitol Reef National Park, Utah. Geomorphology 67, 423–435.
Marcus, M.G., Brazel, A.J., 1992. Summer dust storms in the Arizona Desert. In: Janelle, D.G. (Ed.), Geographical Snapshots of North America. Guilford Press, pp. 411–416.
Matmon, A., Schwartz, D.P., Finkel, R., Clemmens, S., Hanks, T.C., 2005. Dating offset fans along the Mojave section of the San Andreas fault using cosmogenic ^{26}Al and ^{10}Be. Geol. Soc. Am. Bull. 117, 795–807.
Matmon, A., Nichols, K., Finkel, R., 2006. Isotopic insights into smoothening of abandoned fan surfaces, southern California. Quat. Res. 66, 109–118.
Matmon, A., Simhai, O., Amit, R., Haviv, I., Porat, N., McDonald, E., Benedetti, L., Finkel, R., 2009. Desert pavement–coated surfaces in extreme deserts present the longest-lived landforms on Earth. Geol. Soc. Am. Bull. 209, 688–697.
May, J.H., Wells, S.G., Cohen, T.J., Marx, S.K., Nanson, G.C., Baker, S.E., 2015. A soil chronosequence on Lake Mega-Frome beach ridges and its implications for late Quaternary pedogenesis and paleoenvironmental conditions in the drylands of southern Australia. Quat. Res. 83, 150–165.
McAuliffe, J.R., 1994. Landscape evolution, soil formation, and ecological patterns and processes in Sonoran Desert bajadas. Ecol. Monogr. 64, 111–148.
McAuliffe, J.R., Van Devender, T.R., 1998. A 22,000-year record of vegetation change in the north-central Sonoran Desert. Palaeogeogr. Palaeoclimatol. Palaeoecol. 141, 253–275.
McDonald, E.V., Pierson, F.B., F., G.N., McFadden, L.D., 1996. Application of a process-based soil-water balance model to evaluate the influence of Late Quaternary climate change on soil-water movement in calcic soils. Geoderma 74, 167–192.
McDonald, E.V., McFadden, L.D., Wells, S.G., 2003. Regional response of alluvial fans to the Pleistocene-Holocene climatic transition, Mojave Desert, California. Geol. Soc. Am. Spec. Pap. 368, 189–205.
McFadden, L.D., 1988. Climatic influences on rates and processes of soil development in Quaternary deposits of southern California. Geol. Soc. Am. Spec. Pap. 216, 153–178.
McFadden, L.D., Wells, S.G., Dohrenwend, J.C., 1986. Influences of Quaternary climatic changes on processes of soil development on desert loess depositions of the Cima volcanic field, California. Catena 13, 361–389.
McFadden, L.D., Wells, S.G., Jercinovich, M.J., 1987. Influences of eolian and pedogenic processes on the origin and evolution of desert pavements. Geology 15, 504–506.
McFadden, L.D., McDonald, E.V., Wells, S.G., Anderson, K., Quade, J., Forman, S.L., 1998. The vesicular layer and carbonate collars of desert soils and pavements: formation, age and relation to climate change. Geomorphology 23 (2–3), 101–145.
Meadows, D.G., Young, M.H., McDonald, E.V., 2006. Estimating the fine soil fraction of desert pavements using ground penetrating radar. Vadose Zone J. 5, 720–730.
Meadows, D.G., Young, M.H., McDonald, E.V., 2008. Influence of relative surface age on hydraulic properties and infiltration on soils associated with desert pavements. Catena 72, 169–178.
Meek, N., 1989. Geomorphic and hydrologic implications of the rapid incision of Afton Canyon, Mojave Desert, California. Geology 17, 7–10.
Meek, N., 1990. Late Quaternary Geochronology and Geomorphology of the Manix Basin, San Bernardino County, California (Ph.D. Thesis) UCLA, Los Angeles (212 pp.).
Meek, N., 2004. Mojave River history from an upstream perspective. In: Reynolds, R.E. (Ed.), Breaking Up — The 2004 Desert Symposium Field Trip and Abstracts. California State University Fullerton Desert Studies Consortium, Fullerton, CA, pp. 41–49.
Mihir, M., Wasklewicz, T., Liu, T., 2015. Relationship between surface roughness and age of deposits in debris flow fans, Eastern Owens Valley, CA. Geophys. Res. Abstr. 17, EGU2015–EG12444.
Moharana, P.C., Raja, P., 2016. Distribution, forms and spatial variability of desert pavements in arid western Rajasthan. J. Geol. Soc. India 87, 401–410.
Murray, A., Olley, J., 2002. Precision and accuracy in the optically stimulated luminescence dating of sedimentary quartz: a status review. Geochronometria 21, 1–16.
Murray, A.S., Wintle, A.G., 2000. Luminescence dating of quartz using an improved single-aliquot regenerative-dose protocol. Radiat. Meas. 32, 57–73.
Musick, H.B., 1975. The barrenness of desert pavement in Yuma County, Arizona. J. Ariz. Acad. Sci. 10, 24–28.
Naysmith, P., 2007. Extraction and Measurement of Cosmogenic In Situ ^{14}C from Quartz (M.S. thesis) Univerity of Glasgow, pp. 1–86 (http://theses.gla.ac.uk/548/1/2007naysmithmsc.pdf).
Nishiizumi, K., Kohl, C., Arnold, J., Dorn, R., Klein, J., Fink, D., Middleton, R., Lal, D., 1993. Role of in situ cosmogenic nuclides ^{10}Be and ^{26}Al in the study of diverse geomorphic processes. Earth Surf. Process. Landf. 18, 407–425.
Nishiizumi, K., Caffee, M.W., Finkel, R.C., Brimhall, G., Mote, T., 2005. Remnants of a fossil alluvial fan landscape of Miocene age in the Atacama Desert of northern Chile using cosmogenic nuclide exposure age dating. Earth Planet. Sci. Lett. 237, 499–507.
Nishiizumi, K., Imamura, M., Caffee, M.W., Southon, J.R., Finkel, R.C., McAninch, J., 2007. Absolute calibration of ^{10}Be AMS standards. Nucl. Instrum. Methods Phys. Res., Sect. B 258, 403–413.
Oskin, M., Perg, L., Blumentritt, D., Mukhopadhyay, S., Iriondo, A., 2007. Slip rate of the Calico fault: implications for geologic versus geodetic rate discrepancy in the Eastern California Shear Zone. J. Geophys. Res. 112. http://dx.doi.org/10.1029/2006JB004451.
Owen, L.A., Frankel, K., Knott, J.R., Reynhout, S., Finkel, R.C., Dolan, J.F., Lee, J., 2011. Beryllium-10 terrestrial cosmogenic nuclide surface exposure dating of Quaternary landforms in Death Valley. Geomorphology 125, 541–557.
Owen, L.A., Chen, J., Hedrick, K.A., Caffee, M.W., Robinson, A.C., Schoenbohm, L.M., Yuan, Z., Li, W., Imrecke, D.B., Liu, J., 2012. Quaternary glaciation of the Tashkurgan Valley, southeast Pamir. Quat. Sci. Rev. 47, 56–72.
Owen, J.J., Dietrich, W.E., Nishiizumi, K., Chong, G., Amundson, R., 2013. Zebra stripes in the Atacama Desert: fossil evidence of overland flow. Geomorphology 182, 157–172.
Parker, K.C., 1991. Topography, substrate, and vegetation patterns in the northern Sonoran Desert. J. Biogeogr. 18, 151–163.
Peel, R.F., 1960. Some aspects of desert geomorphology. Geography 45, 241–262.
Pelletier, J.D., Harrington, C.D., Whitney, J.W., Cline, M., DeLong, S.B., Keating, G., Ebert, K.T., 2005. Geomorphic control of radionuclide diffusion in desert soils. Geophys. Res. Lett. 32. http://dx.doi.org/10.1029/2005GL024347.
Pelletier, J.D., Cline, M., DeLong, S.B., 2007. Desert pavement dynamics: numerical modeling and field-based calibration. Earth Surf. Process. Landf. 32, 1913–1927.
Perrineau, A., Van DerWoerd, J., Gaudemer, Y., Liu-Zeng, J., Pik, R., Tapponnier, P., Thuizat, R., Rongzhang, Z., 2011. Incision rate of the Yellow River in Northeastern Tibet constrained by ^{10}Be and ^{26}Al cosmogenic isotope dating of fluvial terraces: implications for catchment evolution and plateau building. Geol. Soc. Lond., Spec. Publ. 353, 189–219.
Peterson, F., 1981. Landforms of the Basin and Range Province, Defined for Soil Survey. Nevada Agricultural Experiment Station Technical Bulletin 28.
Peterson, F.F., Bell, J.W., Dorn, R.I., Ramelli, A.R., Ku, T.L., 1995. Late Quaternary geomorphology and soils in Crater Flat, Yucca Mountain area, southern Nevada. Geol. Soc. Am. Bull. 107, 379–395.
Péwé, T.L., 1978. Guidebook to the geology of Central Arizona. Arizona Bureau of Geology and Mineral Technology Special Paper 2.
Phillips, F.M., Zreda, M.G., Evenson, E.B., Hall, R.D., Chadwick, O.A., Sharma, P., 1997. Cosmogenic Cl-36 and Be-10 ages of Quaternary glacial and fluvial deposits of the Wind River Range, Wyoming. Geol. Soc. Am. Bull. 109, 1453–1463.
Pietrasiak, N., Drenovsky, R.E., Santiago, L.S., Graham, R.C., 2014. Biogeomorphology of a Mojave Desert landscape — configurations and feedbacks of abiotic and biotic land surfaces during landform evolution. Geomorphology 206, 23–36.
Pietsch, D., Kuhn, P., 2012. Early Holocene paleosols at the southwestern Ramlat As-Sab'atayn desert margin: new climate proxies for southern Arabia. Palaeogeogr. Palaeoclimatol. Palaeoecol. 365, 154–165.

Pigati, J.S., Lifton, N.A., Timothy Jull, A., Quade, J., 2010. A simplified in situ cosmogenic ^{14}C extraction system. Radiocarbon 52, 1236–1243.
Placzek, C., Granger, D.E., Matmon, A., Quade, J., Ryb, U., 2014. Geomorphic process rates in the central Atacama Desert, Chile: insights from cosmogenic nuclides and implications for the onset of hyperaridity. Am. J. Sci. 314, 1462–1512.
Pope, C.W., 1974. Geology of the Lower Verde River Valley, Maricopa County, Arizona (M.S. thesis) pp. 1–104.
Potter, C., 2016. Mapping changes in desert pavement surfaces of the lower Colorado Desert of Southern California using Landsat time series analysis. Int. J. Adv. Remote Sens. GIS 6, 1747–1754.
Quade, J., 2001. Desert pavements and associated rock varnish in the Mojave Desert: how old can they be? Geology 29, 855–858.
Regard, V., Bellier, O., Braucher, R., Gasse, F., Bourlès, D., Mercier, J., Thomas, J.-C., Abbassi, M.R., Shabanian, E., Soleymani, S., 2006. ^{10}Be dating of alluvial deposits from Southeastern Iran (the Hormoz Strait area). Palaeogeogr. Palaeoclimatol. Palaeoecol. 242, 36–53.
Reheis, M.C., Edwine, J.L., 2008. Lake Manix shorelines and Afton Canyon terraces: implications for incision of Afton Canyon. Geol. Soc. Am. Spec. Pap. 439, 227–259.
Reheis, M.C., Sowers, J.M., Taylor, E.M., McFadden, L.D., Harden, J.W., 1992. Morphology and genesis of carbonate soils on the Kyle Canyon fan, Nevada, U.S.A. Geoderma 52, 303–342.
Rodriguez, M.P., Carretier, S., Charrier, R., Saillard, M., Regard, V., Herail, G., Hall, S., Farber, D., Audin, L., 2013a. Geochronology of pediments and marine terraces in north-central Chile and their implications for Quaternary uplift in the Western Andes. Geomorphology 180-181, 33–46.
Rodriguez, M.P., Carretier, S., Charrier, R., Saillard, M., Regard, V., Herail, G., Hall, S., Farber, D., Audin, L., 2013b. Geochronology of pediments and marine terraces in north-central Chile and their implications for Quaternary uplift in the Western Andes. Geomorphology 180, 33–46.
Rostagno, C.M., Degorgueb, G., 2011. Desert pavements as indicators of soil erosion on aridic soils in north-east Patagonia (Argentina). Geomorphology 134, 224–231.
Sauer, D., Schellmann, G., Stahr, K., 2007. A soil chronosequence in the semi-arid environment of Patagonia (Argentina). Catena 71, 382–393.
Schmidt, S., Hetzel, R., Kuhlmann, J., Mingorance, F., Ramos, V.A., 2011. A note of caution on the use of boulders for exposure dating of depositional surfaces. Earth Planet. Sci. Lett. 302, 60–70.
Shafer, D., Young, M., Zitzer, S., McDonald, E., Caldwell, T., 2004. Coupled environmental processes and long-term performance of landfill covers in the Northern Mojave Desert. DRI Publ. 45203, 1–54.
Sharon, D., 1962. On the nature of hamadas in Israel. Z. Geomorphol. N.F. 6, 129–147.
Shepard, M.K., Arvidson, R.E., Caffee, M., Finkel, R., Harris, L., 1995. Cosmogenic exposure ages of basalt flows - Lunar Crater Volcanic Field, Nevada. Geology 23, 21–24.
Shirahama, Y., Miyairi, Y., He, H., Fu, B., Echigo, T., Kano, K.I., Yokoyama, Y., Ikeda, Y., 2015. Climate-induced changes in sediment supply revealed by surface exposure dating of Sijiquan River terraces, northeastern Tibet. Geomorphology 235, 15–26.
Siame, L.L., Bourles, D.L., Sebrier, M., Bellier, O., Castano, J.C., Araujo, M., Perez, M., Raisbeck, G.M., Yiou, F., 1997. Cosmogenic dating ranging from 20 to 700 ka of a series of alluvial fan surfaces affected by the El Tigre fault, Argentina. Geology 11, 975–978.
Siame, L.L., Sebrier, M., Bellier, O., Bourles, D., Costa, C., Ahumada, E.A., Gardini, C.E., Cisneros, H., 2015. Active basement uplift of Sierra Pie de Palo (Northwestern Argentina): rates and inception from ^{10}Be cosmogenic nuclide concentrations. Tectonics 34, 1129–1153.
Skotnicki, S.J., Young, E.M., Goode, T.C., Bushner, T.C., 2003. Subsurface geologic investigation of Fountain Hills and the Lower Verde River Valley, Maricopa County, Arizona. Arizona Geological Survey Contributed Report CR-03-B, pp. 1–44.
Small, D., Fabel, D., 2016. Was Scotland deglaciated in the Younger Dryas? Quat. Sci. Rev. 145, 259–263.
Sohbati, R., Murray, A.S., Porat, N., Jain, M., Avner, U., 2015. Age of a prehistoric "Rodedian" cult site constrained by sediment and rock surface luminescence dating techniques. Quat. Geochronol. 30, 90–99.
Sohn, M.F., Mahan, S.A., Knott, J.R., Bowman, D.D., 2007. Luminescence ages for alluvial-fan deposits in Southern Death Valley: implications for climate-driven sedimentation along a tectonically active mountain front. Quat. Int. 166, 49–60.
SoilSurveyStaff, 1974. Soil taxonomy. U.S. Department of Agriculture Handbook. 436, pp. 1–754.
Spelz, R.M., Fletcher, J.M., Owen, L.A., Caffee, M.W., 2008. Quaternary alluvial-fan development, climate and morphologic dating of fault scarps in Laguna Salada, Baja California, Mexico. Geomorphology 102, 578–594.
Springer, M.E., 1958. Desert pavement and vesicular layer of some soils of the desert of the Lahontan Basin, Nevada. Proc. Soil Sci. Soc. Am. 22, 63–66.
Stadelman, S., 1994. Genesis and Post-formational Systematics of Carbonate Accumulations in Quaternary Soils of the Southwestern United States (Ph.D Dissertation) Agronomy Department, Texas Tech University, Lubbock, pp. 1–124.
Stirling, M., Ledgerwood, J., Liu, T., Apted, M., 2010. Age of unstable bedrock landforms Southwest of Yucca Mountain, Nevada, and implications for past ground motions. Bull. Seismol. Soc. Am. 100, 74–86.
Stone, J.O., 2000. Air pressure and cosmogenic isotope production. J. Geophys. Res. 105, B23753–B23759.
Sweeney, M.R., McDonald, E.V., Markley, C.E., 2013. Alluvial sediment or playas: what is the dominant source of sand and silt in desert soil vesicular A horizons, southwest USA. J. Geophys. Res. Earth Surf. 118, 257–275.
Symmons, P.M., Hemming, C.F., 1968. A note on wind-stable stone-mantles in the southern Sahara. Geogr. J. 134, 60–64.
Thomas, M.F., Clarke, J.D.A., Pain, C.F., 2005. Weathering, erosion and landscape processes on Mars identified from recent rover imagery, and possible Earth analogues. Aust. J. Earth Sci. 52, 365–378.
Turk, J.L., Graham, R.C., 2011. Distribution and properties of vesicular horizons in the western United States. Soil Sci. Soc. Am. J. 75, 1449–1461.
Turk, J.K., Graham, R.C., 2014. Analysis of sesicular porosity in soils using high resolution X-ray computed tomography. Soil Sci. Soc. Am. J. 78, 868–880.
Turrin, B.D., Dohrenwend, J.C., Drake, R.E., Curtiss, G.H., 1985. K-Ar ages from the Cima volcanic field, eastern Mojave Desert, CA. Isochron West 44, 9–16.
Ugalde, P.C., Santoro, C.M., Gayo, E.M., Latorre, C., Maldonado, S., Pol-Holz, R., Jackson, D., 2015. How do surficial lithic assemblages weather in arid environments? A case study from the Atacama Desert, Northern Chile. Geoarchaeology 30, 352–368.
Ugolini, F.C., Hillier, S., Certini, G., Wilson, M.J., 2008. The contribution of aeolian material to an Aridisol from southern Jordan as revealed by mineralogical analysis. J. Arid Environ. 72, 1431–1447.
Valentin, C., 1994. Surface sealing as affected by various rock fragment covers in West-Africa. Catena 23, 87–97.
Valentine, G.A., Harrington, C.D., 2006. Clast size controls and longevity of Pleistocene desert pavements at Lathrop Wells and Red Cone volcanoes, southern Nevada. Geology 34, 533–536.
Valentine, G.A., Perry, F.V., Krier, D., Keating, G.N., Kelley, R.E., Cogbill, A.H., 2006. Small-volume basaltic volcanoes: eruptive products and processes, and posteruptive geomorphic evolution in Crater Flat (Pleistocene), southern Nevada. Geol. Soc. Am. Bull. 118, 1313–1330.
Van Der Woerd, J., Klinger, Y., Sieh, K., Tapponnier, P., Ryerson, F., Meriaux, A.S., 2006. Long-term slip rate of the southern San Andreas fault from ^{10}Be-^{26}Al surface exposure dating of an offset alluvial fan. J. Geophys. Res. Solid Earth 111. http://dx.doi.org/10.1029/2004JB003559.
Wagner, G.A., Kadereit, A., 2010. Luminescence dating work from the Heidelberg Group: a key technology in geoarchaeology. Mediterr. Archaeol. Archaeom. 10, 3–8.
Wainwright, J., Parsons, A.J., Abrahams, A.D., 1995. A simulation study of the role of raindrop erosion in the formation of desert pavements. Earth Surf. Process. Landf. 20, 277–291.
Wainwright, J., Parsons, A.J., Abrahams, A.D., 1999. Field and computer simulation experiments on the formation of desert pavement. Earth Surf. Process. Landf. 24, 1025–1037.
Wang, W., Dong, Z., Wang, T., Zhang, G., 2006. The equilibrium gravel coverage of the deflated gobi above the Mogao Grottoes of Dunhuang, China. Environ. Geol. 50, 1077–1083.
Wang, F., Michalski, G., Seo, J.-H., Granger, D.E., Lifton, N., Caffee, M., 2015. Beryllium-10 concentrations in the hyper-arid soils in the Atacama Desert, Chile: implications for arid soil formation rates and El Nino driven changes in Pliocene precipitation. Geochim. Cosmochim. Acta 160, 227–242.
Ward, D.J., Cesta, J.M., Galewsky, J., Sagredo, E., 2015. Late Pleistocene glaciations of the arid subtropical Andes and new results from the Chajnantor Plateau, northern Chile. Quat. Sci. Rev. 128, 98–116.
Wells, P.V., 1983. Paleobiogeography of montane islands in the Great Basin since the last glaciopluvial. Ecol. Monogr. 53, 341–382.
Wells, S.G., Dohrenwend, J.C., McFadden, L.D., Turrin, B.D., Mahrer, K.D., 1985. Late Cenozoic landscape evolution on lava flow surfaces of the Cima volcanic field, Mojave Desert, California. Geol. Soc. Am. Bull. 96, 1518–1529.
Wells, S.G., McFadden, L.D., Poths, J., Olinger, C.T., 1995. Cosmogenic ^{3}He surface-exposure dating of stone pavements: implications for landscape evolution in deserts. Geology 23, 613–616.
Wilcox, M.K., Wood, J.M., Tromble, J.M.`., 1988. Factors influencing infiltrability of semiarid mountain slopes. J. Range Manag. 41, 197–206.
Williams, S., Greeley, R.D.N.T.M., 1984. NASA T-86246, 1, 169–170. Desert Pavement Study at Amboy, California. NASA Tech Memo TM-86246 1, pp. 169–170.
Williams, S.H., Zimbelman, J.R., 1994. Desert pavement evolution: an example of the role of sheetflood. J. Geol. 102, 243–248.
Williams, A.J., Buck, B.J., Soukup, D.A., Merkler, D.J., 2013. Geomorphic controls on biological soil crust distribution: a conceptual model from the Mojave Desert (USA). Geomorphology 195, 99–109.
Wood, J.D., Graham, R.C., Wells, S.G., 2002. Surface mosaic map unit development for a desert pavement surface. J. Arid Environ. 52, 305–317.
Wood, Y.A., Graham, R.C., Wells, S.G., 2005. Surface control of desert pavement pedologic process and landscape function, Cima Volcanic field, Mojave Desert, California. Catena 59, 205–230.
Wright, R.H., Hall, N.T., Hanson, K.L., Sharp, W.D., Klein, J.J.P., Nichols, H.J., Mote, T.I., Keischer, T.C., Ruffell, K.M., 2014. Uranium-series ages of faulted alluvial fan deposits, Mesquite Regional Landfill, southeastern California. Environ. Eng. Geosci. 20, 199–224.
Young, M.H., McDonald, E.V., Caldwell, T.G., Benner, S.G., Meadows, D.G., 2004. Hydraulic properties of a desert soil chronosequence in the Mojave Desert, USA. Vadose Zone J. 3, 956–963.
Zerboni, A., 2008. Holocene rock varnish on the Messak plateau (Libyan Sahara): chronology of weathering processes. Geomorphology 102, 640–651.
Zhang, W., Tan, L., Zhang, G., Qiu, F., Zhan, H., 2014. Aeolian processes over gravel beds: field wind tunnel simulation and its application atop the Mogao Grottoes, China. Aeolian Res. 15, 335–344.
Zimmerman, S.G., Evenson, E.B., Gosse, J.C., Erskine, C.P., 1994. Extensive boulder erosion resulting from a range fire on the type-Pinedale moraines, Fremont Lake, Wyoming. Quat. Res. 42, 255–265.
Zreda, M.G., Phillips, F.M., Kubik, P.W., Sharma, P., Elmore, D., 1993. Cosmogenic ^{36}Cl dating of a young basaltic eruption complex, Lathrop Wells, Nevada. Geology 21, 57–60.